Insights into G-Quadruplex–Hemin Dynamics Using Atomistic Simulations: Implications for Reactivity and Folding

Petr Stadlbauer[1,2]*, Barira Islam[1§], Michal Otyepka[1,2], Jielin Chen[3], David Monchaud[4], Jun Zhou[3], Jean-Louis Mergny[1,3,5] and Jiří Šponer[1]*

[1] Institute of Biophysics of the Czech Academy of Sciences, Královopolská 135, 612 65 Brno, Czech Republic.
[2] Regional Centre of Advanced Technologies and Materials, Faculty of Science, Palacký University, Šlechtitelů 27, 771 46 Olomouc, Czech Republic.
[3] State Key Laboratory of Analytical Chemistry for Life Science, School of Chemistry & Chemical Engineering, Nanjing University, Nanjing 210023, China.
[4] Institut de Chimie Moléculaire (ICMUB), CNRS UMR6302, UBFC Dijon, 21078, France.
[5] Laboratoire d'Optique et Biosciences, Ecole Polytechnique, CNRS, INSERM, Institut Polytechnique de Paris, 91128 Palaiseau cedex, France.
[§] Present address: Department of Pharmacy, School of Applied Sciences, University of Huddersfield, Huddersfield HD1 3DH, United Kingdom
* corresponding authors

ABSTRACT

Guanine quadruplex nucleic acids (G4s) are involved in key biological processes such as replication or transcription. Beyond their biological relevance, G4s find applications as biotechnological tools since they readily bind hemin and enhance its peroxidase activity, creating a G4-DNAzyme. The biocatalytic properties of G4-DNAzymes have been thoroughly studied and used for biosensing purposes. Despite hundreds of applications and massive experimental efforts, the atomistic details of the reaction mechanism remain unclear. To help select between the different hypotheses currently under investigation, we use extended explicit-solvent molecular dynamics simulations to scrutinize the G4/hemin interaction. We found that besides the dominant conformation in which hemin is stacked atop the external G-quartets, hemin can also transiently bind to the loops and be brought to the external G-quartets through diverse delivery mechanisms. Importantly, the simulations do not support several mechanistic possibilities (*i.e.*, the wobbling guanine and the iron-bound water molecule) but rather suggest tentative mechanisms in which the external G-quartet itself is responsible for the unique H_2O_2-promoted biocatalytic properties of the G4/hemin complexes. Our simulations show that once stacked atop a terminal G-quartet, hemin rotates about its vertical axis while readily sampling shifted geometries where the iron transiently contacts oxygen atoms of the adjacent G-quartet. This dynamics is not apparent from the ensemble-averaged structure. We also visualize transient interactions between the stacked hemin and the G4 loops. Finally, we investigated interactions between hemin and on-pathway folding intermediates of the parallel-stranded G4 fold. The simulations suggest that hemin drives the folding of parallel-stranded G4s from slip-stranded intermediates, acting as a G4 chaperone. Limitations of the MD simulation technique are also briefly discussed.

KEYWORDS

DNAzyme; DNA folding; DNA ligand; Molecular dynamics simulations

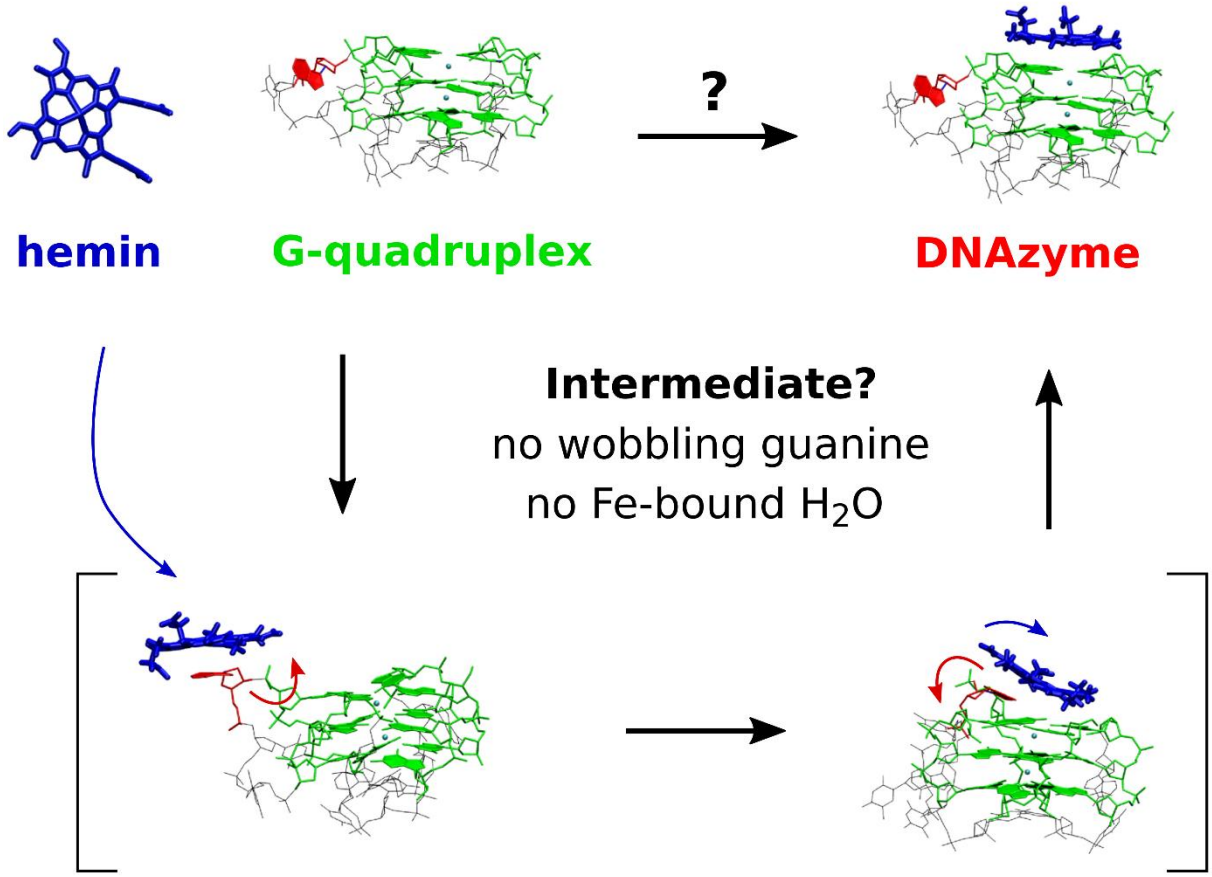

Graphical Abstract. Hemin can bind to G-quadruplex via loop-assisted delivery. The catalytically active structure does not seem to contain an iron-bound water molecule sandwiched in between hemin and G-quadruplex or wobbling guanine.

INTRODUCTION

Guanine quadruplexes (G4s) are undoubtedly the most studied non-canonical nucleic acid structures. G4s are quadruple helices that fold from both DNA and RNA guanine (G)-rich sequences and adopt a variety of topologies depending on their nucleotide sequence and experimental conditions.[1-2] The basic unit of G4 is a quartet of guanines (G-quartet), in which guanines are H-bonded in a cyclic arrangement (Figure 1).[3] G4s are created when at least two quartets stack upon each other to form a G-stem, which creates a channel running through its whole length, with inwardly pointing guanine O6 atoms that chelate cations (*e.g.*, K^+) and further stabilize the overall G4 architecture. G4 topology is characterized by structural rules comprising *syn*/*anti* conformations of guanines, strand directionality and loop types, which lead to a large topological diversity when combined.[4-6]

Potential G4-forming sequences are widespread in the genome (>700,000 sequences),[7-8] which lends credence to key G4 roles in cell's life and functions.[1-2, 9] This prevalence makes them active players in – and attractive targets for – genetic diseases including cancers[10-11] and neuropathologies.[12-13] G4s bind numerous ligands,[14] including porphyrinic derivatives such as hemin (Fe(III)-protoporphyrin IX), which endows the resulting G4/hemin complex with unique catalytic properties referred to as G4-DNAzyme.[15] The formation and H_2O_2-promoted peroxidase activity of G4-DNAzymes has found many applications notably as biosensors and for green chemistry purposes.[16-19] G4-DNAzymes might also be relevant *in vivo* as heme is a naturally occurring cofactor involved in a variety of cellular processes. As intracellular heme levels vary in pathological conditions, G4-DNAzyme is hypothesized to cause oxidative damage to DNA.[20] Alternatively, G4 might sequester free heme to protect cells against free heme-mediated toxicity.[21]

Despite dozens of applications now developed with G4-DNAzymes, structural information on the G4/hemin complexes is still fragmentary and the exact catalytic mechanism remains elusive. NMR experiments show the preferential stacking of hemin atop the 3′-quartet of parallel-stranded G4s.[22-24] However, the dynamic aspect of G4-hemin binding has not been thoroughly addressed to date. The actual G4-DNAzyme mechanism is currently debated. Only recently, electron paramagnetic resonance spectroscopy (EPR) has indicated formation of Compound I (hemin cation-radical with oxygen bound to iron) as a reactive intermediate, which suggests a similarity to the horseradish peroxidase reaction mechanism (Figure 1).[25] Various hypothetical hemin activation mechanisms have been postulated, involving either a water molecule sandwiched in between the hemin and the adjacent quartet,[26-29] the O6 atom of a wobbling guanine from the adjacent G-quartet,[30] or a guanine from a slipped G4.[31] All these catalytic intermediates rely on an oxygen or nitrogen atom as an activating axial ligand of the iron atom, but none of them has been unambiguously confirmed (Figure 1). In addition, reaction rate enhancements have been observed for G4 precatalysts with flanking bases[31-35] or when free nucleotides are added in the reaction solutions,[36-37] possibly because they help with binding and activation of H_2O_2 in proximity of hemin iron (Figure 1).

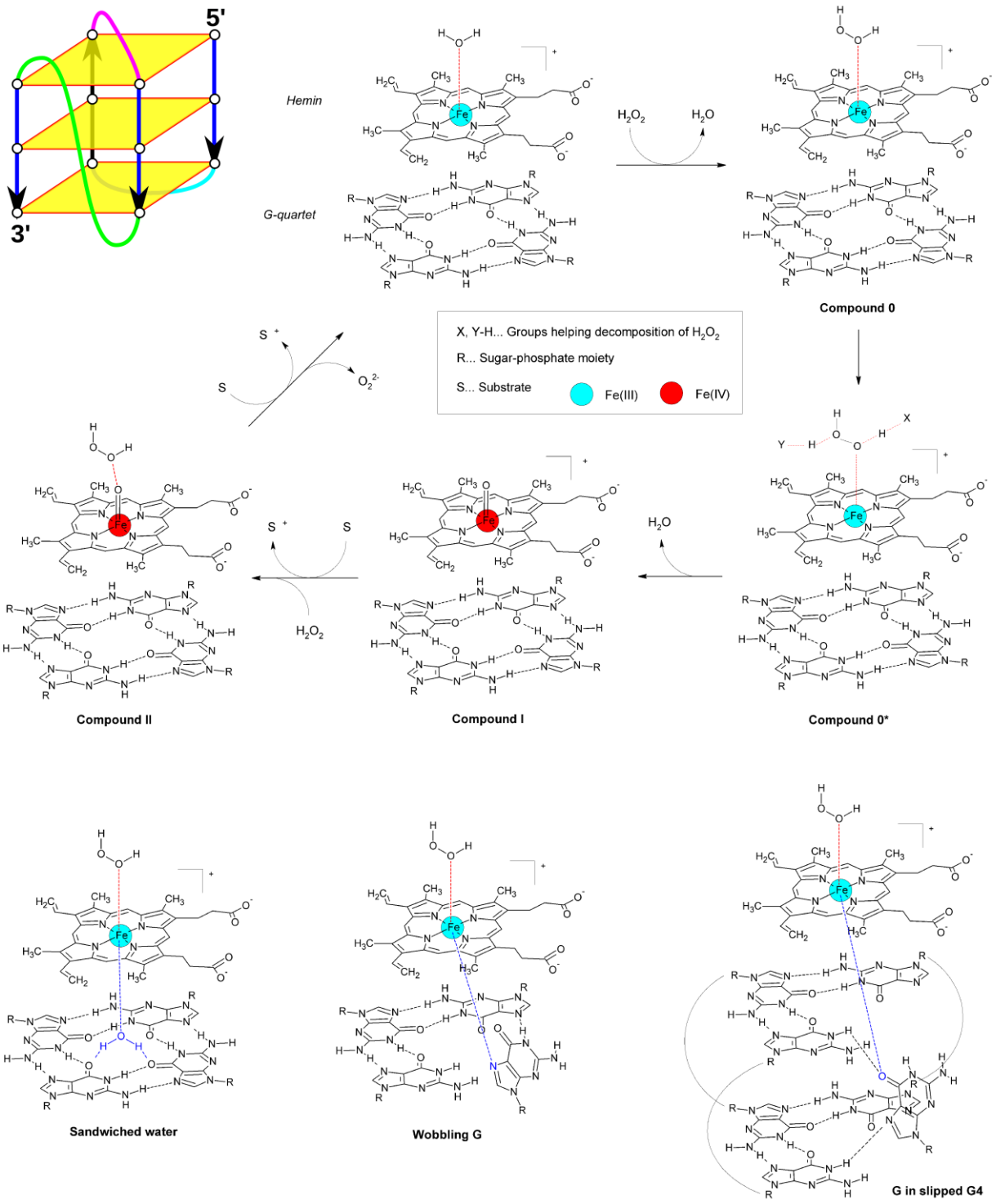

Figure 1. G4 structure, G4-hemin peroxidase cycle, and suggested hemin axial ligands. (Top left) G4 is formed by a G-stem, which is composed of stacked planar G-quartets (yellow; each composed of four Gs). Strands of the G-stem (blue) may be connected by loops: propeller (green), diagonal (purple) and lateral (cyan) are most common. (Middle) G4's terminal G-quartet may bind hemin and form a DNAzyme with peroxidase activity. Its expected mechanism is thought to be similar to horseradish peroxidase and key steps are shown in the figure. (Bottom) Axial ligands of iron in hemin bound to G4 suggested so far in the literature, shown at the Compound 0 state.[26-31]

The G4-hemin interactions may also affect the G4 folding process. Recent studies suggest that G4s might follow intricate folding pathways best characterized by kinetic partitioning.[38-42] Such a folding process is thought to be dominated by competition between diverse long-living G4 folds resulting from a combination of *syn*- and *anti*-oriented Gs.[39] Many other structures can act as short-living transitory species during the folding process;[42-43] in this line, MD simulations suggest an astonishingly large variety of structures that can participate in the G4 folding.[39] The diversity of the structures and the expected large separation of time-scales between residency times of the metastable structures and transition times of active structural rearrangements make detection of transitory species by experimental techniques very challenging, opening space for advanced simulation studies.[42-43] The G4 folding process may start with a very fast first phase resulting in an initial population of diverse G4 folds as long-living species.[42-43] This population then equilibrates[38-39, 44-46] over long time periods, often days,[38, 41, 47-48] while some of the thermodynamically less stable but kinetically more accessible G4s act as long-living kinetic traps. Given the long time scale of the whole folding process, biologically relevant conformations of G4-forming sequences may differ from those in equilibrium.[39, 47] In this context, ligands may substantially affect the complex G4-folding landscapes.[49-50]

Generally, transitions between different G4 topologies seem to require partial or complete unfolding of individual molecules. There is, however, one exception. Key folding intermediates of parallel-stranded all-*anti* G4s may correspond to transiently-populated slipped G4s with a reduced number of quartets.[51-53] Transitions between such structures can occur without any unfolding of the G-stem, through vertical strand-slipping movements. Although this process appears straightforward, experiments indicate that some slip-stranded structures can have long lifetimes for G4s with GGGG or longer G-tracts.[54] Role of slip-stranded structures of parallel G4s has been considered in several recent experimental folding studies.[55-56] As many ligands featuring a flat aromatic structure, including hemin, interact with (and seem to support) parallel-stranded G4s,[57-58] they may affect the folding process, stabilizing some of the intermediates and/or modulating structural rearrangements.

In light of the unique catalytic properties of the G4/hemin complexes, we wonder whether the interactions of hemin with some of the folding intermediates could contribute to the G4-DNAzyme peroxidase activity.[31] We thus used extensive all-atom explicit-solvent MD simulations to explore several aspects of the G4/hemin interaction. Our results show how hemin binds to parallel-stranded G4s and how the loops contribute to the binding process through an unprecedented delivery mechanism. We propose conformations that might contribute to the G4-DNAzyme catalytic activity and provide an explanation for the observed difference in activity of G4s with short loops, long loops and flanking nucleotides. Finally, we simulate partially folded slip-stranded parallel G4s complexed with hemin to investigate whether such intermediates can contribute to the overall catalytic activity and to understand how a ligand binding event may affect G4-folding pathway.

METHODS

Starting structures. We selected two intramolecular parallel-stranded all-*anti* G4s: the human telomeric G4 d[A(GGGTTA)$_3$GGG] (PDB ID: 1KF1, X-ray structure; Figure 2),[59] and d[TAGGGCGGGAGGGAGGGAA] (PDB ID: 2LEE, solution NMR structure, first frame).[60] 1KF1 contains three three-nucleotide-long propeller loops and 2LEE contains three single-nucleotide-long propeller loops, and both G4s contain purine and pyrimidine bases in the loops. To assess how hemin interacts with bare G4 and possibly with its loops, we removed all the 5′- and 3′-flanking nucleotides. For binding simulations we placed a hemin molecule without bound axial ligands at a random position around the G4. We generated 20 starting positions for 1KF1 and 10 for 2LEE; the starting distance between G4 and hemin varied from

contact distance to 40 Å with respect to the G4 center of mass (Supporting Figure S1). For 1KF1, we also prepared three starting positions at a distance of about 80 Å.

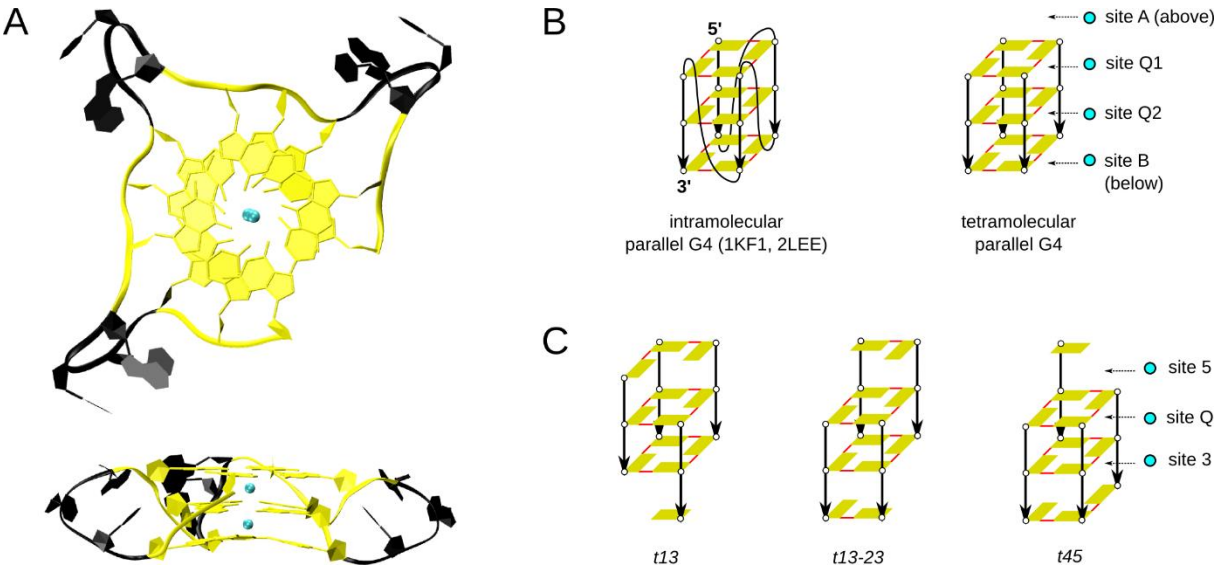

Figure 2. **Starting structures in MD simulations**. (A) top and side view of structure of the parallel-stranded G4 1KF1 (5′-flanking adenine present in the crystal structure was removed). The G-stem is depicted in yellow, TTA loops are shown in black, and potassium cations bound in the channel are cyan. (B) schemes of the intramolecular parallel-stranded G4s, and the tetramolecular parallel-stranded d[GGG]$_4$ G4, shown along with designation of the channel binding sites. (C) d[GGG]$_4$ G4s with one or more slipped strands, named as *t13*, *t13-23*, and *t45*, along with designation of the channel binding sites. Slip-stranded structures were suggested to act as late-stage folding/formation intermediates of parallel-stranded all-*anti* G4s.[51-53] The schemes in panels (B) and (C) and in next figures are drawn as follows: guanines are yellow; a pair of H-bonds between two guanines is depicted by a red line; the sugar-phosphate backbone is depicted by a black arrow showing the 5'→ 3' progression; loop nucleotides and channel cations are not shown; bound hemin will be shown as a cyan rectangle (not present in this figure).

To assess whether a water molecule can act as a hemin-coordinating ligand and occupy a putative binding site between the hemin and the G4 channel, we took the simulated 1KF1 structure with hemin bound either atop the 5′- or the 3′-quartet, removed the three TTA loops to create a three-quartet tetramolecular d[GGG]$_4$ G4, and manually placed a water molecule in between the G4 and hemin. We also studied the hemin interaction with slip-stranded d[GGG]$_4$ G4s: to this end, we took the d[GGG]$_4$ G4 as described above and we manually prepared structures with slipped strands by removal and addition of Gs at appropriate ends, so that a G4 with two quartets was created. In doing so, we prepared three different structures (Figure 2), one with a strand slipped in the 3′-direction, designated *t13* (meaning tetramolecular G4, nominally slipped strand *1* in the 3′-direction), one with two neighboring slipped strands (*t13-23*, i.e. slipped strand *1* in the 3′-direction and strand *2* in the 3′-direction) and one with a strand slipped in the 5′-direction (*t45*; we use *t45* name instead of equivalent *t15* to better visually differentiate from *t13*). These three structures were simulated with and without bound hemin with initially three cations in the channel, at sites 5, Q, and 3 (Figure 2). Some simulations with 5′-bound hemin were initiated with only two channel cations, with the site 5 vacant.

MD simulations. Each system was solvated in an octahedral box of SPC/E water molecules with the distance between solute and box border of at least 10 Å.[61] When required by the hemin initial position, the box was enlarged to ensure that the hemin-G4 distance across the box border (to its periodic image) was at the desired length. Hemin and G4 concentration was about 0.01M in most simulations. The simulation box was neutralized by K^+ ions and then 0.15M KCl[62] was added. Where intended, cations were placed inside the G4 channel. We applied the latest AMBER OL15 DNA force field.[63] OL15 includes also several earlier modifications[64-66] of the Cornell *et al*. force field.[67-68] The overall combination of force-field parameters appears to be presently optimal for G4 simulations.[69] GAFF with Shahrokh's parameters was applied for hemin.[70] The preparation was done in the leap module of AMBER16.[71] Solvated structures were subjected to equilibration following standard protocol, described in Supporting Information. Production phase was performed in the CUDA version of pmemd module of AMBER16.[71-73] SHAKE and SETTLE algorithms were used to constrain covalent bonds involving hydrogen.[74-75] Hydrogen mass repartitioning scheme was used with integration time step set to 4 fs.[76] Electrostatics was treated by the PME method and the cut-off for non-bonding interactions was set to 9 Å.[77-78] Pressure was held at 1 bar and temperature at 300 K using the weak-coupling method.[79] For the sake of completeness, in three simulations dedicated to study kinetics of hemin-to-G4 association we used Langevin thermostat with a collision frequency of 2 ps^{-1} and Monte Carlo barostat. The reason for change of the thermostat is merely our decision to update our simulation protocol and these were the last simulations done for this study. We have recently compared both thermostats in G4 simulations and they appear to provide equivalent results.[80]

Length of individual simulations varied from 0.5 to 5 microseconds as specified in Table 1.

Table 1. **List of simulations.**

Simulated G4	Hemin, water and ions initial position	Length (μs)[a]	Outcome summary
1KF1	Hemin randomly placed up to 40 Å away from the G4	20 × 5	Hemin bound to 5'-quartet in 80% of the cases, in 20% to 3' quartet; loop bases **may** contact hemin iron in the final pose
1KF1	Hemin randomly placed at around 80 Å from the G4	2 × 2, 3.5, 0.9[b], 1.6[b], 3.7[b]	Hemin binding to G4 is diffusion-driven
2LEE	Hemin randomly placed up to 40 Å away from the G4	10 × 2	Hemin bound to 5'-quartet in 80% of the cases, in 20% to 3' quartet; loops **do not** contact hemin iron in the final pose
$d[GGG]_4$[c]	Hemin bound to the 5'-quartet	4 × 5	Stable
$d[GGG]_4$[c]	Hemin bound to the 5'-quartet, water between hemin and G4	5 × 0.5	G4 stable, water expelled on average within 89 ns
$d[GGG]_4$[c]	Hemin bound to the 3'-quartet	5 × 5	Stable
$d[GGG]_4$[c]	Hemin bound to the 3'-quartet, water between hemin and G4	4 × 1, 2	G4 stable, water expelled on average within 759 ns
t13	Hemin bound to the 5'-triplet, 3 K^+	1, 3.5, 3 × 5	Stable
t13	Hemin bound to the 5'-triplet, water between the triplet and quartet, 2 K^+	1.5, 2 × 2, 2.9, 3.5	Stable; water replaced by K^+ in two simulations
t13	Hemin bound to the lone 3' G, 3 K^+	5 × 5	3 × strand slippage to full three-quartet G4 with *syn* 5' quartet; 1 × strand slippage to *t45;* 1 × lone G bulged out (may then contact hemin iron) with hemin stacked to quartet

t13	No hemin	5 × 5	Stable, but the 5'-triplet flipped to *syn*
t13-23	Hemin bound to the 5' G:G pair, 3 K^+	4 × 5	3 × strand slippage to *t13;* 1 × to full three-quartet G4
t13-23	Hemin bound to the 5' G:G pair, water between the G:G pair and quartet, 2 K^+	0.8, 2, 2.3, 3.6, 5	4 × strand slippage to *t13;* 1 × to full three-quartet G4; water replaced by K^+ in all simulations
t13-23	Hemin bound to the 3' G:G pair, 3 K^+	5 × 5	Stable, but 5' G:G pair flipped to *syn*
t13-23	No hemin	5 × 5	2 × stable; 1 × unfolded; 2 × strand slippage to *t13; 5′* G:G pair flipped to *syn*
t45	Hemin bound to the lone 5' G, 3 K^+	5 × 5	2 × strand slippage to *t13;* 3 × lone G bulged out (may then contact hemin iron) with hemin stacked to quartet
t45	Hemin bound to the lone 5' G, water between the G and quartet, 2 K^+	5	Lone G bulged out (may then contact hemin iron) with hemin stacked to quartet, no sandwiched water
t45	Hemin bound to the 3' G-triplet, 3 K^+	5 × 5	Stable
t45	No hemin	5 × 5	2 × strand slippage to *t13-23;* 3 x strand slippage to *t25-45*; 5' G:G pair in *t13-23* and *t25-45* flipped to *syn*

[a] Multiple times (*n* × ...) means *n* independent simulations of a given system, *e.g.*, "4 x 1, 2" notation means four independent 1 μs-long simulations and one 2 μs-long simulation.
[b] Langevin thermostat with Monte Carlo barostat.
[c] Complete all-*anti* parallel-stranded three-quartet G4 stem.

RESULTS

We have accumulated 433 μs of MD trajectories; their length and brief overall outcome are summarized in Table 1.

Hemin binds to both 5′- and 3′-quartets. In the 20 simulations performed with 1KF1 and 10 simulations performed with 2LEE, hemin spontaneously bound to the two external G-quartets, according to three typical pathways: hemin could *i*- move directly to stack on the terminal quartets; *ii*- first make pre-binding to the loops and then be transferred to the stacked conformation by a conformational change of the loop; or *iii*- first interact transiently with the loops, be released back into the bulk solvent and then make another binding attempt. Regardless of the exact details of the binding process, in all simulations hemin eventually bound to the terminal quartets and stayed there until the end of simulation. For both 1KF1 and 2LEE, hemin bound to the 3′- and 5′- quartet in ~20% and ~80% of simulations, respectively (Figure 3A).

Interception of the free hemin by 1KF1 G4, which contains three-nucleotide propeller loops, happened mostly *via* stacking to the loops. We observed four direct binding events to the 5′-quartet, three to the 3′-quartet, thirteen quartet stacking events mediated by the loops and nineteen transient bindings to the loops, after which the hemin departed back to the bulk. The three loops were involved in the binding approximately equally. As the three-nucleotide loops are flexible, we observed hemin stacking to a single base, formation of two-base stacking platforms, intercalation between two bases, as well as interaction with the grooves (Supporting Figure S2). Hemin usually remained bound to the loops for hundreds to thousands of ns, before it either unbound or slid to the 5′-quartet. A typical process looked like as if adenine (A) "picked hemin up" and delivered it to the 5′-quartet (Figure 3B; Supporting Movie SM1): hemin first stacked on the loop's A, then the loop underwent a conformational change and A with bound hemin moved above the 5′-quartet. Finally, hemin contacted the quartet and the A left the stacking position on the quartet, so that the hemin could stack atop the quartet through its entire surface (Figure 3B). No such hemin delivery

process was found at the 3′-side, though we evidenced a single event in which hemin bound to a thymine (T) slid along the backbone to the 3′-quartet.

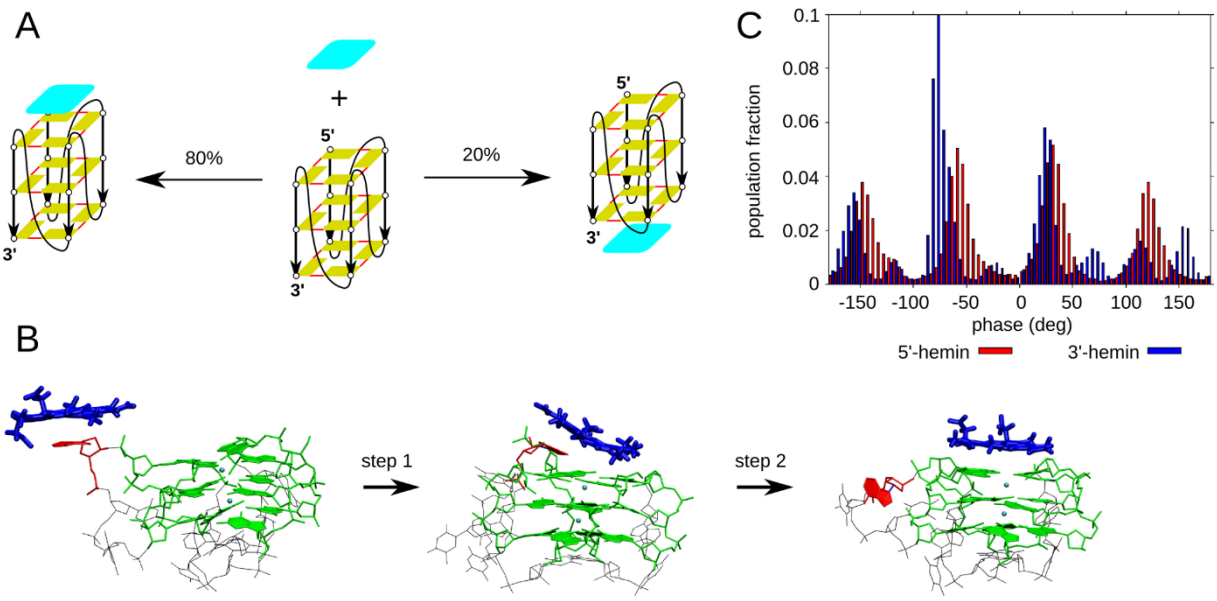

Figure 3. **Binding of hemin to 1KF1 G4**. A) In all simulations hemin ended up bound either to the 5′- or 3′-terminal quartet, with a 4:1 probability ratio, similarly to the 2LEE simulations. The schematic representation is explained in the legend to Figure 2. B) Adenine-assisted transfer of hemin to the 5′-quartet; hemin is shown in blue, the involved adenine in red, the G-stem is in green and other loop nucleotides appear in black. Once the first step happens, the second step is fast and takes only a few ns. The whole process is visualized in Supporting Movie SM1. C) Rotational positioning of hemin stacked on terminal quartets is not uniform. Four-modal distribution was observed for hemin bound to 5′-quartet, and eight-modal to 3′-quartet. Bin width was set to 5 deg. The phase is an arbitrarily chosen dihedral angle defined by the following four points: 1) Center of mass of C1′ atoms of G2 and G20 (*i.e.*, guanines of the middle quartet from the first and last G-stretch), 2) center of mass of base heavy atoms of guanines forming the middle quartet, 3) hemin Fe(III), 4) hemin ring hydrogen atom located between the two carboxyethyl side chains.

We performed six large-box simulations with a distance between the hemin and the 1KF1 G4 of about 80 Å to ensure no initial interaction. We observed three direct bindings to the 5′-quartet, one direct binding to the 3′-quartet, and two loop binding events after which hemin was transferred to the 5′-quartet. Besides that, we observed two temporary binding events, one to a loop and one to the open groove without loop. The picture is thus consistent with the smaller-box simulations. Using the average time for binding to a quartet t and the concentration of hemin and G4 in a given simulation box c, using the formula $k = 1/t/c$, the rate of binding would be estimated on the order of 10^9 M^{-1} s^{-1}, *i.e.*, diffusion-driven (Supporting Table S1).

With 2LEE G4, hemin could bind directly to the terminal G-quartets or, more frequently, use pre-binding to the loops. We observed two direct bindings to the 5′-quartet, two to the 3′-quartet, six deliveries from the loops to the 5′-quartet and six transient bindings to the loops. Hemin bound only to either A8 or A12, but never to C4, probably due to its smaller stacking surface and also smaller sampling in the 2LEE simulation set (Supporting Figure S3). When bound to either of the As, hemin remained stacked usually for a few

hundreds of ns, before it either unbound or slid from A to the 5′-quartet. Only direct binding events were found for the 3′-quartet.

Dynamics of the bound hemin and its interactions with loop residues. Once stacked atop a terminal G-quartet, hemin rotated about its vertical axis. Since hemin has two sidechains and G4 has a sugar-phosphate backbone protruding from the plane of the terminal G-quartets, a four-modal distribution was found for hemin stacked on the 5′-quartet and eight-modal distribution for the 3′-quartet in 1KF1 (Figures 3C and Supporting Figure S4). The split from four- to eight-modal distribution was likely due to the interaction with the sugar rings exposed below the 3′-quartet. Hemin was not rigidly aligned exactly above the center of G4 stem, but rather wobbling around it due to thermal fluctuations (Figure 4A). The movement was more limited with hemin stacked atop the 3′-quartet. Adenines from TTA loops could rarely, and very briefly (at most a few ns), stack atop the hemin/G4 complex and form an A/hemin/5′-quartet sandwich. Interestingly, Ts located near the 3′-quartet could also form a similar sandwich (Figure 4B), whose formation was found more frequent than the 5′-quartet sandwich. The average frequency of formation was a few times per microsecond (counting only simulation time when hemin is stacked on the 3′-quartet) and the T(O4)-iron direct contact time was up to dozens of ns, which would extend up to hundreds of ns if considering just the proximity of iron (6 Å). Therefore, the 1KF1/hemin complex allows for loop bases to appear in the vicinity of hemin central iron atom with a greater chance when hemin is stacked on the 3′-quartet.

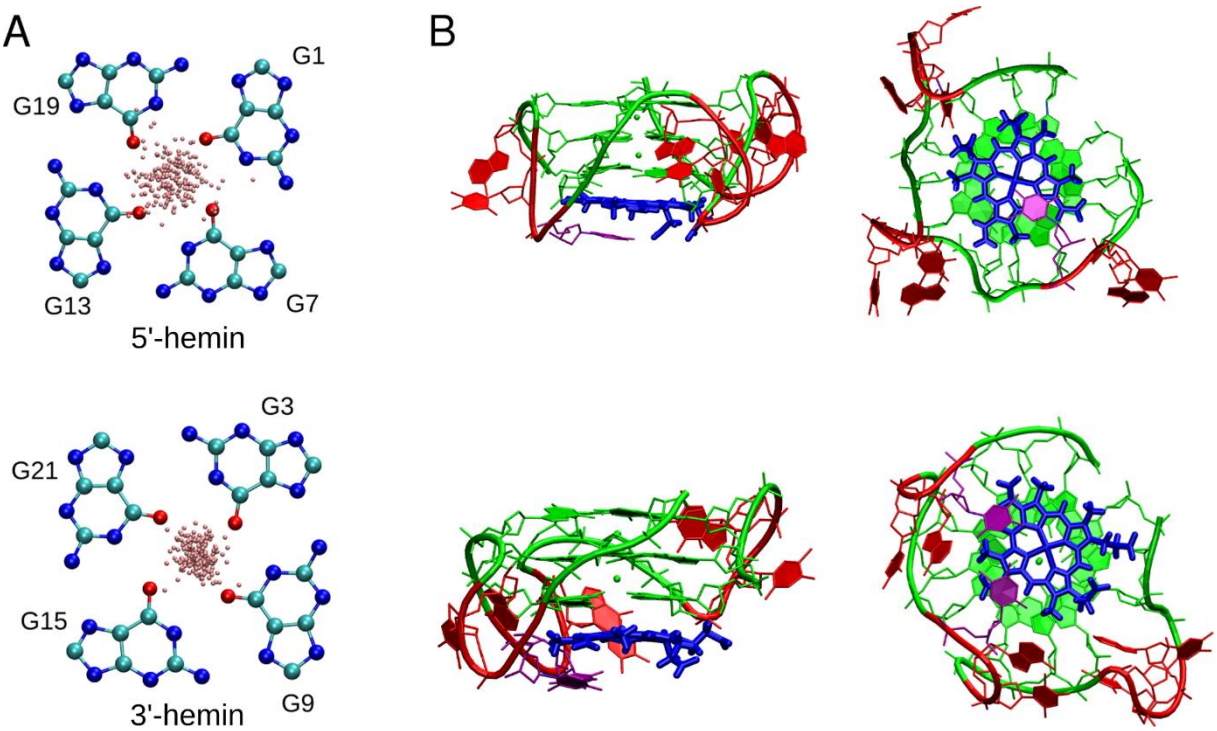

Figure 4. **Hemin bound to the terminal quartets of 1KF1**. (A) 200 randomly selected positions of the iron atom (pink) above the 5′- and 3′-quartet. (B) Iron in the center of hemin may occasionally be contacted by one of the loop thymines – structure with one thymine (top; two views) and structure with a T:T base pair (bottom; two views). Hemin is blue, the thymine(s) in the vicinity of iron purple, G-stem green and other loop nucleotides red.

When bound to either of the 2LEE terminal G-quartets, hemin rotated with a four-modal distribution, caused by steric clashes between the hemin sidechains and the G4 sugar-phosphate backbone (Supporting Figures S5 and S6). No 1KF1-like eight-modal distribution

for 3′-binding was observed, because the short loops made the backbone shaped differently than in 1KF1. The wobbling movement of hemin around the G-stem axis was observed again. Due to steric constraints, none of the single-nucleotide loops could stack, even transiently, above or below the hemin to form a sandwich-like structure and reach the central iron atom of hemin. Therefore, the hemin rotation was not affected, and, more importantly, the loops' bases are unlikely to contribute to the catalytic properties of the G4/hemin system, should the reactive conformation be the one with hemin fully stacked on G4.

No water molecule remained trapped between freshly stacked hemin and the terminal G-quartet in any of the binding simulations. All water molecules moving around were always expelled before hemin fully stacked atop the quartet. No ion exchanges of the two channel cations bound inside the G-stem of 1KF1 and 2LEE with the bulk were observed.

A water molecule between the hemin and the G4 is expelled. Subsequently, simulations of the tetramolecular G4 (d[GGG]$_4$) with bound hemin were performed. The G4 was entirely stable in all simulations while hemin was again rotating about its vertical axis (Supporting Figures S7, S8 and S9). When stacked to the 5′-quartet, the rotation had a four-modal distribution (Figures S7 and S9). Hemin was again wobbling around the G4 axis. Two K^+ ions remained in the channel at sites Q1 and Q2 (see Figure 2) at all times; no ion exchanges were observed. With hemin stacked on the 3′-quartet, the rotation was characterized by a four-modal distribution (Figures S8 and S9), with four main peaks and four shoulders (Figure S9).

Since we did not observe any water molecule spontaneously occupying the space in between the hemin and the G4 in our simulations, we carried out ten simulations starting with a water molecule manually placed between the d[GGG]$_4$ and either the 5′- (water at site A) or the 3′-stacked hemin (site B). In all simulations performed with the 5′-stacked hemin, the water molecule quickly (within 1-286 ns) escaped into bulk, while the lifetimes were longer with the 3′-stacked hemin (217-1018 ns). The water molecule always left the G4 by transient incorporation into the terminal quartet *via* H-bonding,[80] which was followed by a quick (order of ns) expulsion to the groove. Within the force-field approximation, the binding of a water molecule in between the hemin and the G4 is thus a very unlikely event, even if we do not have any estimate of its free-energy penalty (as no water binding event was observed). The different expulsion times at 5′- and 3′- ends may be explained by different G-quartet buckling: in both 1KF1 and the related d[GGG]$_4$, both in the crystal structures and in the simulations, the 5′-quartet is nearly perfectly flat even without stacked hemin; the 3′-quartet without stacked hemin is buckled towards the G4 center (Supporting Figure S10), and hemin binding makes it flat. However, in the simulations with a water molecule initially placed at site B, the buckling re-occurs and the water molecule has thus a little more available space.

Hemin stabilizes slipped G4s and may accelerate transition to the complete stem. Next, we simulated hemin bound to slip-stranded G4s, suggested late-stage on-pathway intermediates in folding of parallel-stranded G4s.[39, 51-52] The goal was two-fold, *i*- to see if some slip-stranded structures can sample potential catalytically potent geometries (*i.e.*, geometries with hemin stacked to a not-fully-exposed quartet or with base functional groups in proximity of the iron) and *ii*- to get insights into the influence of binding of a flat ligand on the folding landscape. To simplify the calculations we used the minimal d[GGG]$_4$ construct, however, the studied strand-slippage movements are fully relevant to complete intramolecular G4s.[52-53] We used three structures and two positions for hemin, which together with simulations lacking hemin resulted into nine starting states, sufficiently though not completely representing the part of folding landscape represented by slip-stranded structures.

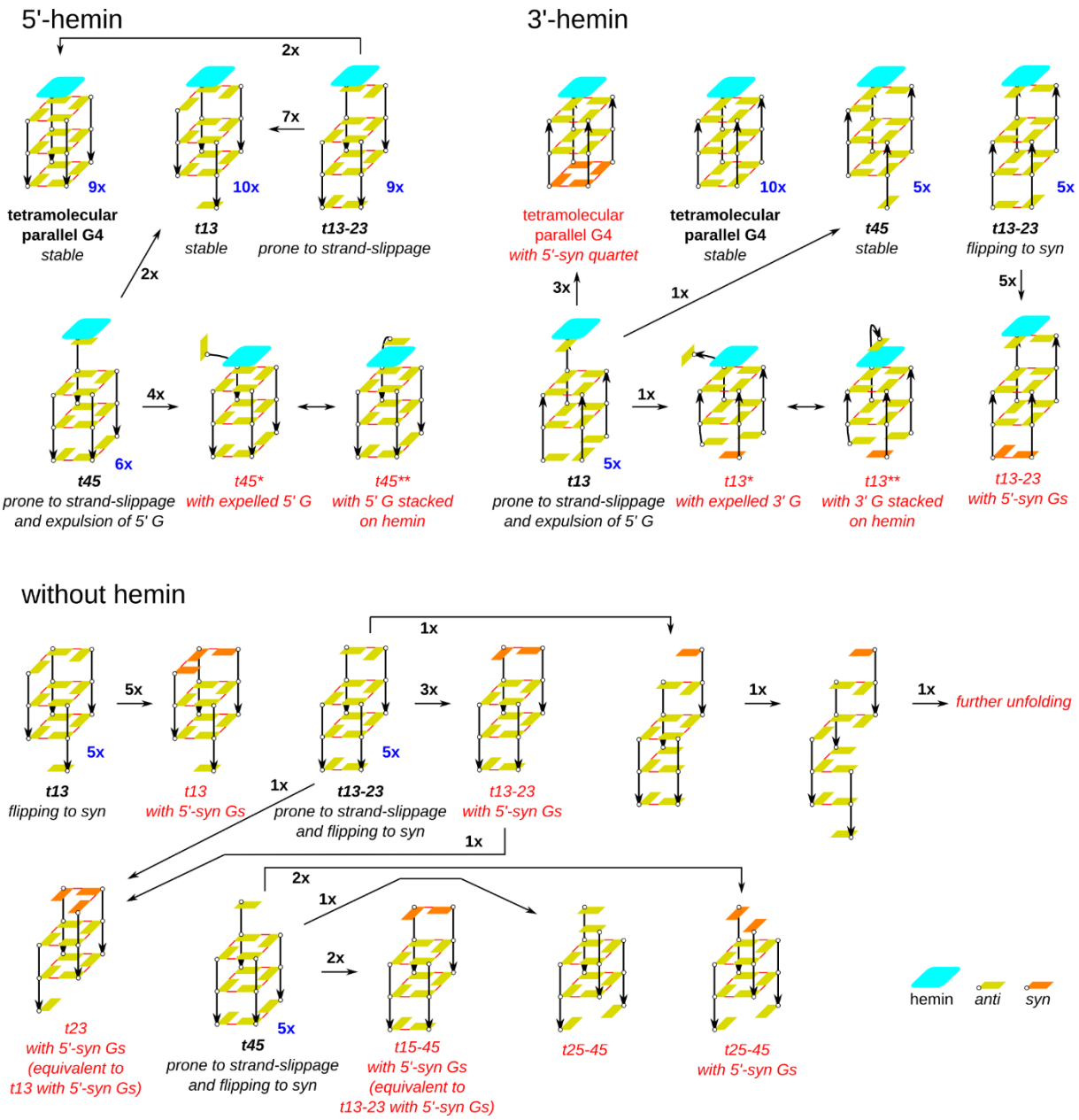

Figure 5. **Rearrangements in complexes of tetramolecular G4s with and without hemin**. Black font denotes structures used as starting structures while the red ones occurred spontaneously in simulations. Arrows show transitions observed in our simulations. The blue numbers next (bottom right) to structural schemes indicate the number of simulations initiated from a given starting structure, while the black numbers at the arrows count transitions seen in the dataset of 74 simulations. The structures marked with asterisks behave like a G4 with a flanking base near hemin. The complexes with 3′-stacked hemin are shown upside down to emphasize similarity of 5′-hemin-*t45* with 3′-hemin-*t13* and also of 5′-hemin-*t13* with 3′-hemin-*t45*. "Further unfolding" marked in this scheme is shown in Supporting Figure S12. The schematic representation is explained in the legend to Figure 2.

Development of all simulations is succinctly summarized in Figure 5. Comparison of all results reveals that the presence of hemin stabilizes slip-stranded on-pathway intermediates of folding of the parallel all-*anti* G-stem and accelerates reduction of strand-slippage towards the full three-quartet G-stem. In more details:

a. *t13* with hemin stacked on the 5′-G-triplet: this complex was fully stable in all five simulations with three K^+ (at sites 5, Q, and 3). Hemin was not aligned above the *t13* central axis but shifted towards O6 atoms, and this shift was visible even in the ensemble-averaged position, as it improves stacking with the triplet (Figure 6A). The characteristic fast hemin rotation about its vertical axis is mostly stopped in *t13* by the formation of two stable H-bonds between either of the two hemin negatively-charged carboxylate groups and the Gs' imino and amino hydrogens of the vacant Watson-Crick edge of the G-triplet (Figure 6B). The carboxylate group also provided its oxygen to the channel K^+, replacing the oxygen atom from the missing guanine. These two H-bonds may also contribute to the shift of hemin off the G4 axis. They were occasionally disrupted, allowing hemin to rotate again until another H-bond formation occurred. The carboxylate group involved in the H-bonds served as a steric hindrance and prevented *t13* from strand slippage and formation of a complete three-quartet G4 on our simulation time scale. No exchange of the two ions present in the initial structure at sites Q and 5 with the bulk was observed, while a weak cation binding occurred at site 3. In five additional simulations starting without a cation at site 5, a cation was captured from bulk solvent in two of them; in the three other simulations, however, the site remained unoccupied. The G-triplet then adopted a cyclic triangular arrangement of the three Gs (Figure 6C), likely due to the absence of cation or a water molecule at site 5.

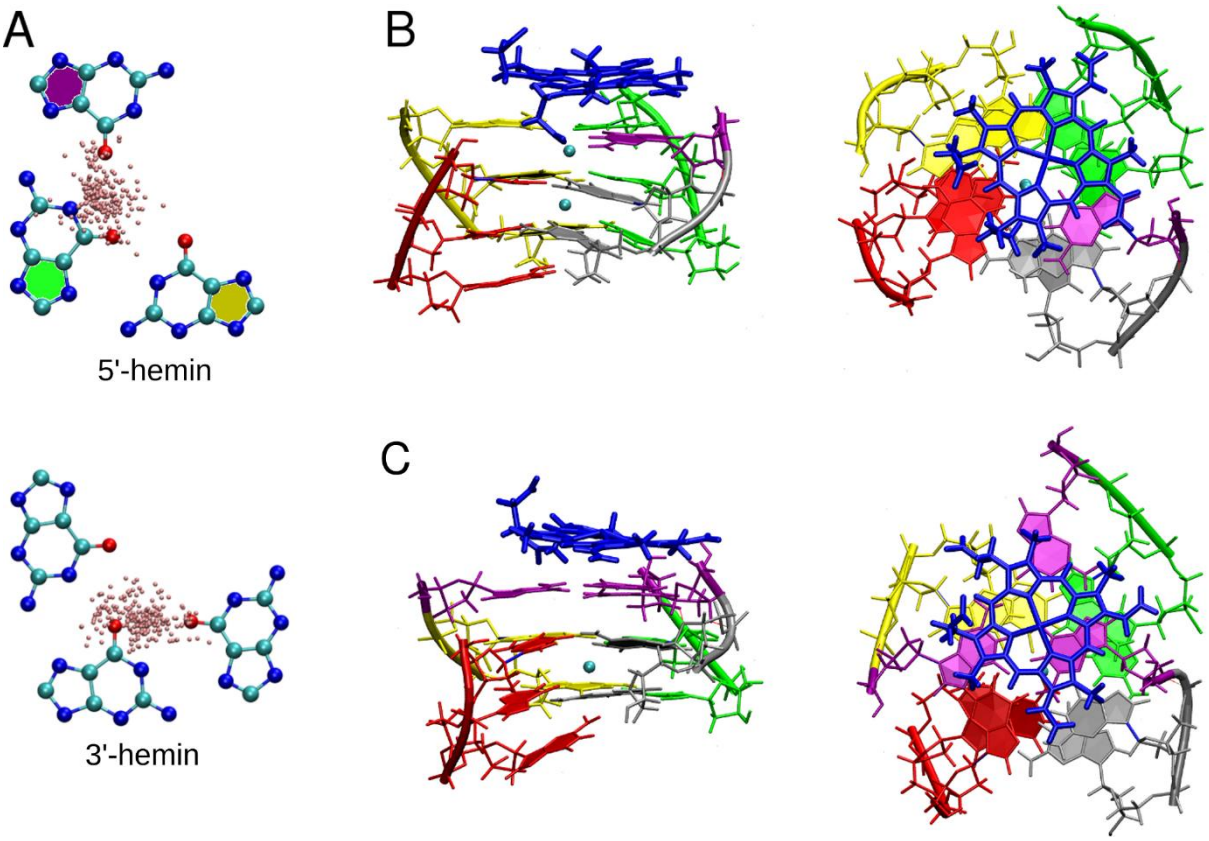

Figure 6. **Hemin bound to the G-triplet of *t13* and *t45***. (A) 200 random positions of the iron atom (pink) above the 5′-triplet of *t13* and the 3′-triplet of *t45* (B) 5′-hemin/*t13* complex. Two H-bonds with one of the guanines of the G-triplet beneath are formed via flexible carboxyethyl side chain. The carboxylate group also coordinates the channel cation. The ligand is visibly shifted towards the triplet, as also seen in panel A. (C) 5′-hemin/*t13* complex with the 5′-triplet under hemin in the cyclic triangular shape. In panel A, top figure, nucleotides are marked by the same color as in the structure in panel B. In panels B and C, hemin is blue while each G-strand is shown in a different color. Channel cations are cyan. In

panel B, G involved in the H-bonding is shown in purple; in panel C, the three Gs forming the triangular triplet are shown in purple.

b. *t13-23* with 5′-stacked hemin: this complex was prone to strand slippage (Figure 5), which occurred in all four simulations (with three K^+) after only a few dozens to hundreds of ns. The products were either the *t13* structure (three times) or the complete three-quartet G4 (once) formed by a simultaneous strand slippage of two strands (Supporting Movie SM2). Even two of the events leading to *t13* initiated as a double-strand slippage, but full upward movement of one of the strands was hindered by the above-described H-bonds between the hemin and a G below it. The cations at sites Q and 5 were stable in this set of simulations, while the cation at site 3 left after the simulation start. Weak cation binding at site 3 remained in only one simulation. In the set of five simulations starting with only two channel cations (at sites Q and 3), formation of *t13* was observed (four times) or the *t13-23* structure remained stable (once). The strand slippage events appeared dozens to thousands of ns after the simulation start. The Q-site cation was stable; site 5 became occupied by K^+ after 30-300 ns and site 3 usually lost the cation upon binding of K^+ at site 5.

c. *t45* with 5′-stacked hemin: this complex provided the richest dynamics among the complexes with 5′-stacked hemin (Figure 5). Hemin contacted the exposed parts of the top G-quartet within the first few ns of the five simulations with three K^+. Then either strand slippage to *t13* occurred within hundreds of ns (twice), or the lone 5′-G was pushed out (three times) to allow hemin to fully stack on the top G-quartet, in a process that resembled the last two steps of the hemin delivery assisted by A in the 1KF1 binding simulations (Figure 3B). Before the lone G was bulged out, hemin spent a considerable time (10, 14 and 80 ns) in a tilted orientation in which it was still stacked with the top G but also in contact with two exposed Gs of the quartet below. In this position, the central iron was in vicinity of the lone G's O6 atom (Supporting Figure S11). The dislodged lone G was then mostly moving around in the bulk solvent, but occasionally could stack on top of the hemin molecule to form a sandwich-like structure. In each of the three simulations, we observed about a dozen events in which the G was in the vicinity of the iron, which lasted up to dozens of ns. This behavior was similar to the dynamics of A in the 1KF1 TTA loops, but was more frequent. In the only simulation starting with two K^+, we also observed expulsion of the lone G. The *t45* simulations thus revealed two contradicting trends: *i*- the route towards *t13* should accelerate the G4 folding, while *ii*- the formation of the structure in which hemin was sandwiched between the G-stem and the lone 5′-G can trap the slip-stranded structure. The exact kinetic balance between these two processes, however, cannot be elucidated from the simulations. In all simulations, only two cation binding sites were occupied, with two possible scenarios: *i*- the cation at site 5 left the G4; or *ii*- the cation at site 3 left the G4 and both remaining cations (at sites Q and 5) relocated one level downwards upon stacking of hemin to the 5′-quartet, so that the final outcome was same as in the first scenario. Infrequent (less than one per microsecond) cation exchanges with the bulk occurred at site 3.

d. *t13* with 3′-stacked hemin: this complex resembled that of *t45* with 5′-stacked hemin and likewise it exhibited the most diverse behavior (Figure 5). Three different scenarios were observed:

i- cations at sites 3 and 5 were expelled immediately after the start of the simulations (three times) and hemin tilted, being simultaneously stacked on the 3′-lone G and in contact with two Gs of the adjacent G-quartet. The slipped strand was (within 70-220 ns) pushed in the 5′-direction to complete the three-quartet stem. In addition, all the 5′-Gs flipped into the *syn* conformation, so that a three-quartet G4 with an all-*syn* 5′-quartet was formed, along with a cation capture from bulk to occupy site 5 (eventually becoming Q1). Such an *anti*-to-*syn* rearrangement was already observed in simulations performed with tetramolecular G4s[69] and

was explained by presence of the 5′-terminal OH groups.[81] The *syn* preference of the 5′-terminal Gs is due to the formation of an internal H-bond between the 5′-terminal OH and the N3 in the base.[81-83] All *anti*-to-*syn* rearrangements reported in this study should be viewed in this context. They are typical for G4s with 5’-terminal Gs but much less likely for intramolecular G4s and for tetramolecular G4s with 5′-flanking nucleotides.

ii- a cation left site 5 immediately after the simulation start but, unlike in the previous case, hemin did not adopt the tilted position. It remained stacked on the 3′-lone G (until 240 ns) and then a double strand slippage took place (320 ns) to morph *t13* into *t45*. The movement of the fourth strand was blocked by a hemin carboxylate group that formed H-bonds with the lone 3′-G; the H-bonds remained in the newly formed G-triplet and slowed down the rotation of the hemin.

iii- the hemin tilted right after the beginning of the simulation and the 3′-lone G was expelled (210 ns). Similarly to *t45* with 5'-stacked hemin, the dislodged G either moved in the solvent or stacked on the other side of the hemin, forming a sandwich (the preferred state) in which the G could readily reach the hemin iron atom and stay there for hundreds of ns, which is considerably longer than with the *t45*. One G from the 5′-triplet flipped into the *syn* conformation.

e. *t13-23* with 3′-stacked hemin: this complex was structurally stable, except that the two non-quartet 5′-Gs adopted a *syn* conformation (Figure 5). The absence of slippage is consistent with the fact that vertical strand movement in G-stems with a combination of *syn* and *anti* Gs would result in a steric clash.[52] Hemin either rotated about its vertical axis (twice) or was blocked (thrice). In the five simulations, no cation exchange with the bulk occurred at sites Q and 3, while weak cation binding with multiple exchanges was observed at site 5. The resulting dynamics thus differed from the complex of *t13-23* with hemin at the 5′-end where strand slippage occurred, because flipping of 5′-terminal Gs into *syn* was blocked by hemin.

f. *t45* with hemin stacked on the 3′-triplet: these simulations provided outcomes comparable to simulations performed with hemin stacked atop the 5′-triplet of *t13* (Figure 5), *i.e.*, the system was stable in all five simulations. Formation of the H-bonds between the hemin carboxylate groups and the Watson-Crick edge of the G-triplet was observed, but, unlike the 5′-hemin/*t13* complex, hemin almost freely rotated around its vertical axis. Still, it was shifted away from the G4 axis (Figure 6A). Flipping of the lone 5′-G into the *syn* conformation was observed only once, because the lone G never de-stacked from the adjacent quartet in any of the simulations, therefore it did not have a chance to flip; in the only case of *syn* occurrence, it was not the base, but the sugar that turned upside down to form an internal H-bond.

h. slip-stranded G4s without hemin. Finally, a series of simulations was performed with a slip-stranded tetramolecular G4s without hemin (Figure 5), which are described, for space reasons, in the Supporting Information. Comparison of all results reveals that the presence of hemin stabilizes slip-stranded on-pathway intermediates of folding of the parallel all-*anti* G-stem and accelerates reduction of strand-slippage towards the full three-quartet G-stem.

DISCUSSION

Non-covalent association of G4s and hemin provides complexes endowed with an interesting catalytic activity that has been particularly exploited for performing peroxidase-mimicking biotransformations. Understanding the reaction mechanism is a necessary step for optimizing both the G4 scaffolds and hemin-related cofactors. Here, we have performed 433 μs of MD simulations to shed light into hemin binding to parallel-stranded G4 and its possible folding intermediates, with four interrelated goals: *i*- to decipher how hemin interacts with G4, *ii*- to gain insights into G4 dynamics, especially loop dynamics, upon hemin binding, *iii*- to assess

whether hemin can affect the G4 folding landscape, mainly *via* the interaction with slip-stranded G4 folding intermediates, and *iv*- to identify which structure(s), be it a hemin/full-G4 complex or any of the G4 intermediates, could be catalytically active. It is obvious that MD simulations alone cannot describe the catalytic mechanisms. However, they can provide insights narrowing the options and suggest new possibilities.

What is the axial ligand of hemin? Some studies tentatively suggested that there is an axially coordinated water molecule sandwiched between heme(Fe(II)) and G4[26-29] or cobalt(III)porphyrin and G4.[84] However, to our opinion, the presence of the water molecule does not seem to be unambiguously proven yet for several reasons. NMR signals of an alleged water molecule in heme-G4 complexes are broad, which the authors attributed to exchange of the water molecule with bulk solvent.[27] However, while the water exchange cannot be ruled out, we think it would mean that either the complex is labile or that G4 is fragile, otherwise there is no route by which a water molecule could enter/escape from the small cavity between G4 and stacked heme. We reported here that a water molecule can be *expelled* from the channel through the quartet after manual insertion between the G4 stem and bound hemin. It occurs because of the enormous strain in the simulated structure that is unable to find any suitable position for the water molecule. The opposite process (opening the quartet and shuffling a bulk water molecule into the G-stem through a reversed pathway) is very unlikely, especially when the upper quartet is stabilized by a flat ligand. Also the signal's integral intensity casts doubt on how many hydrogens actually correspond to the "water" signal. Unfortunately, hemin-G4 complexes evade direct NMR characterization because of the paramagnetic properties of Fe(III).[22] Contribution from a state in which the ligand is not tightly bound to the quartet interface cannot be excluded. Raman[26] and EPR[25] spectroscopic analyses of hemin-G4 complexes support the transient formation of a hexa-coordinate iron, but without providing clues on the nature of the ligands. As for the NMR signals, unbound hemin could possibly contribute to the result. The structure of a heme-G4 complex with a water molecule in between hemin and G4 was also investigated theoretically by DFT calculations. However, with a distance between G4 and hemin of 3.5 Å, guanine carbonyl oxygens were suspiciously pushed away from the quartet plane by the proximal water,[27] indicating a substantial strain (steric clash) in the structure. Since the QM and QM/MM calculations do not allow sampling comparable to MD simulations to sufficiently relax the starting structures, there is a risk that these calculations are performed on unrealistic (high-energy) structures.[85] Finally, resolved crystal structures of salphen complexes stacked to 3′-quartet of a G4 do not reveal any ligand sandwiched between nickel(II) or copper(II) and G4 (PDB id's 3QSF and 3QSC, respectively).[86] When considering all systems discussed in this paragraph, one should also bear in mind that the results obtained with non-hemin systems (including heme(Fe(II)) instead of hemin) may not reflect properties of the hemin-G4 complex.

Collectively, the simulations performed here do not support the picture of the sandwiched water molecule, mostly because of a series of steric conflicts. We admit that fully accurate modelling of the interaction of water with iron is beyond the current limits of simulation methodology. A water molecule in proximity of the iron would become strongly polarized and its properties would change dramatically, which is not possible to capture by a non-polarizable force field (see the section "Force field limitations" in Supporting Information). However, the expulsion of water molecules in the simulations is so decisive that it is unlikely to be solely due to force-field limitations. No water molecule remained in the site upon hemin binding and if placed manually, it was expelled quickly.

Irrespective of the simulation results we also argue that if the iron axial ligand was a water molecule, the actual role of the G4 would be questionable, unless there is very specific, yet unknown electronic interplay in the hemin-water-G4 system. The fact that a buried water

molecule would not exchange with other molecules does not make the system, in our opinion, far different from free hemin in water. Alternatively, the axial ligand could be a sterically smaller hydroxide anion, which would in many experiments be undistinguishable from ordinary water. We have performed tentative QM/MM computations and the preliminary results actually suggest that hydroxide anion is more suitable to be bound in this position than a water molecule (data not shown).

Another hypothesis found in the literature is that one of the four Gs of the G-quartet adjacent to hemin is wobbling (tilted) and provides its O6 atom as an axial ligand to the iron (Figure 1).[30] The simulations performed here do not support such mechanism as well. A wobbling guanine would be associated with a large energy penalty due to its partial unstacking from both the adjacent quartet and the hemin and a partial breaking of H-bonds within its G-quartet. The simulations showed that the quartet adjacent to hemin is almost perfectly flat, while without hemin, the 3′-quartet is buckled into the G4 stem (Figure S10). Recent experiments with isoguanine quartets and quintets also suggested that planar arrangement is required for reactivity.[87] However, tilted guanines could be provided by slip-stranded G4s (see below).

We alternatively suggest that the quartet itself could be the sought-for axial ligand. Although the ensemble-averaged structure gave the expected alignment of iron atom with the channel, hemin dynamically fluctuated around the G4 axis, sampling positions closer to the G's O6 atoms (Figure 4A). Diverse structures with shifted hemin were readily sampled in contrast to structures with wobbling G or a buried water molecule. Therefore, any of the four carbonyl oxygens could be the source of electrons for iron coordination. One could argue that there is a lack of electron density for this mechanism to be efficient, because each G's carbonyl oxygen is involved in a hydrogen bond with a neighboring G and coordinates a K^+ in the channel. However, the model with water sandwiched between hemin and G4 might have a similar problem. It assumes presence of two hydrogen bonds between the water and carbonyl oxygens, and thus enough electron density from the carbonyl oxygens in the direction of hemin (Figure 1). We also note that internal G-quartets in the G-stem contain Gs forming hydrogen bonds with neighboring Gs and coordinate *two* proximal K^+ in the channel. This indicates that a G-quartet can coordinate chemical species both above and below its plane concomitantly.

Alternatively, the mere interaction of hemin with the electron-rich aromatic surface of the G-quartet could somehow enhance the reactivity *per se*. For example, hemin can bind to graphene and the complex was reported to enhance the peroxidase reaction about hundred times.[88-89] Hemin bound to graphene oxide affects the peroxidation rate, too; either slightly increasing (up to about four times) or decreasing it depending on the experimental conditions and the degree of oxidation of graphene.[90-92] Given the similarity of graphene (oxide) surface and a G-quartet surface, both peroxidase reactions could be enhanced by the electron-rich aromatic system. Such a model is not fully in line with the existence of a hexa-coordinate iron (provided the EPR spectra reflect the actual reactive geometry) but could be rationalized by the concomitant stacking of hemin atop the quartet and coordination of iron by the four proximal carbonyl oxygens, which could act as the sixth ligand. In principle, some such stacking-caused effect could work with other suggested ligands, such as the sandwiched water or hydroxide anion, too; i.e., these mechanisms are not mutually exclusive.

Our simulations further suggest that some reactive conformations could correspond to G4-folding intermediates, chiefly the slip-stranded G4s. For example, the studied *t13*, *t13-23*, and *t45* structures (Figure 2) have a G's O6 atom in the vicinity of the iron; in the complexes with 5′-bound hemin, the angle at which the O6 interacted with the iron increased from *t13*, where hemin and G are nearly parallel (Figure 6B), to *t45*, in which hemin is tilted considerably (Figure S11). The trend was opposite in the complexes with 3′-bound hemin.

Nevertheless, although such complexes may in principle be reactive (in line with the wobbling G hypothesis), they are certainly rarely populated with respect to the dominant state with G-quartet-hemin stacking. However, they could be sampled more frequently than structures of unperturbed G4 stem with wobbling G. Notably, the potential reactive conformations in slip-stranded G4s suggested by our simulations are very different from the one tentatively contemplated before (Figure 1).[31] Similarly, the axial ligand could be transiently provided by the loops, as the simulations show that loop bases, as well as Gs of slip-stranded intermediates, might be temporarily sandwiched between a quartet and tilted hemin (Figures 3B, 5 and S11). For the sake of completeness, stacking of hemin with a triad of slip-stranded structures may increase capability of the structure to incorporate a water molecule, though we have not seen this in the present set of simulations.

Loops and flanking bases may bind H_2O_2 in the vicinity of the hemin iron atom. Catalytic activity of G4/hemin complex can be further enhanced by loop/flanking nucleotides, which act as a general acid-base during the initial step of the reaction.[31-34, 93] Our simulations provide solid evidence to support this model: the three-nucleotide propeller loops of 1KF1 and single slipped Gs in *t13* and *t45* (being positioned equivalently to flanking nucleotides) are flexible enough to form a base/hemin/quartet sandwich (Figures 4B and 5). In this arrangement, the base is close to the hemin iron atom thus being suited to bind H_2O_2, stabilizing the transition state of the reaction and increasing its rate. The sandwich could be formed at both 5′- and 3′-ends of the G4/hemin complex. The single-nucleotide propeller loops are too short to form this type of sandwich, as demonstrated by our simulations with 2LEE. This is in line with experimental data showing no rate enhancement by short loops.[31] This result seems to be convincingly demonstrated within the limits of the MD simulation technique.

Hemin binding process. We initiated many of our simulations with a hemin floating in the bulk solvent and witnessed multiple binding events to G4s. In both 1KF1 and 2LEE, hemin often first bound to the G4 loops and not directly to the accessible G-quartets of the G4s. A greater versatility of intermediates was obtained with the longer loops of 1KF1 as compared to the short loops of 2LEE, but all of them were characterized by hemin stacking on bases (Figures S2 and S3). The three-nucleotide loops can adopt various conformations capable of binding hemin, stacking either to a single base or to transiently formed base pairs and even triplets. The single-nucleotide loops provide hemin with two faces of the single base only. A dynamic equilibrium makes hemin prone to detach from the loops back to the bulk solvent, or to be transferred from the loops to the 5′-quartet (Figure 3B, Supporting Movie SM1). Surprisingly, we did not observe such a hemin delivery by loop bases to the 3′-quartet, neither in 1KF1 nor 2LEE. This highlights how internal dynamics of the loops might play a major role in the binding process. It is possible (although it has not been seen in our simulations due to the affordable simulation timescale) that contacts with the loops may also facilitate the hemin unbinding events. Spontaneous binding of a ligand to the loops, direct binding to terminal G-quartets and sliding of ligands from the loops along the backbone to the terminal G-quartets has been observed in MD simulations of G4s with other ligands, including telomestatin and BRACO19.[94-100] A decisive loop-assisted delivery of RHPS4 to the partially exposed 3′-quartet of the human telomeric hybrid-1 type G4 has been reported, in which the propeller loop with bound ligand significantly changed its conformation and brought the ligand closer to the quartet (*Cf.* Supplementary Movie “Hybrid_G4_2HY9_02” in ref.[95]), but, to the best of our knowledge, direct loop-to-quartet ligand delivery that we observed in our study has not been reported yet. Once hemin bound to either the 5′- or 3′-quartet, either directly from the solvent or after being delivered by the loop, it stayed stacked on the G-quartet until the end of the simulations.

5′- *vs*. 3′-quartet hemin binding. Hemin is thought to prefer binding to the 3′-quartet of G4 with telomere-mimicking and some other sequences.[22-24, 31-32] It may seem contradictory to our simulations, in which ~80% preference is given to the 5′-quartet binding of the 1KF1 G4. However, our simulations are not in thermodynamic equilibrium and our time scale is insufficient to see events such as hemin unstacking from the quartets, precluding accurate estimations of the equilibrium constants. Considering the MD-estimated k_{on} in the order of 10^9 M^{-1} s^{-1} (Table S1) and a measured K_D in the range of μM[31] would lead to k_{off} in the range of 10^3 s^{-1}. It is well within the time-scales of experimental setups, thus, binding – unbinding events are definitely affecting experimental outcomes. It is therefore possible that the 5′-quartet preference is a kinetically driven process possibly enhanced by the loop conformational behavior, which brings hemin to the 5′-quartet. The 3′-quartet binding could be the thermodynamically preferred binding mode, provided that the 3′-end binding has smaller off-rate. Such process is orders of magnitude beyond the simulation time scale. Furthermore, our simulations have shown that the hemin binding is a multi-pathway process and that the binding pose is an ensemble of structures differing in hemin rotation and loop nucleotides position. It would complicate a reliable quantitative calculation of binding free energies by some enhanced-sampling methods (for discussion of the limitations of enhanced-sampling methods see, *e.g.*, ref.[101]).

Hemin may increase G4-folding rates. G4-folding is a complex process, which likely involves stable off-pathway intermediates (basins), presumably misfolded G4s. These long-living kinetic traps significantly slow down the G4 folding and contribute to kinetic partitioning.[39, 42] Under these circumstances, ligands may speed up the G4 folding process by stabilizing certain on-pathway intermediates pertinent to the native basin. In the case of the parallel-stranded G4s, substantial involvement of on-pathway structures with slipped strands has been proposed.[51-53] Flat ligands may promote their formation compared to off-pathway intermediates, reducing the kinetic partitioning, speeding up reduction of strand slippage and stabilizing the complete parallel-stranded G4. Although the full folding is far beyond the simulation time scale, our results provide indirect support to the above considerations: comparison of simulations with and without hemin showed that the ligand exerts the aforementioned effects within the folding funnel pertinent to the parallel-stranded all-*anti* G4 state (Figure 5). Strand slippage is a movement in which an entire G-stretch of a given G4 slides by one quartet level downwards or upwards;[51-52] such movements are hindered for G4s with mixture of *syn* and *anti* Gs, thus being specific to parallel G4s. We can assume that hemin stacking stabilizes structures with the largest stacking areas, *i.e.*, it favors G-quartets, and thus promotes strand slippage in the direction of complete three-quartet parallel G4s. Our simulations of slip-stranded intermediates (Figure 5) indeed showed that, in absence of hemin, strand movements commonly occur in the direction towards disruption of the structure, while in the presence of hemin (specifically when atop the 3′-quartet of *t13* and the 5′-quartet of *t13-23* and *t45*), the same slipped G4s always rearrange in the direction towards the complete G4 (Supporting Movie SM2). In addition, the time required for initiation of strand movements was shorter in simulation of slipped G4s with bound hemin. Finally, the full three-quartet $d[GGG]_4$ with hemin is very rigid in simulations while without hemin it shows some volatility to strand slippage.[102]

Therefore, hemin may act as a chaperone for parallel G4s, as already demonstrated for several other G4 ligands.[103] These results corroborate our recent investigations in which we described major stabilizing effects of hemin on parallel-stranded intramolecular G-triplexes,[43] making them plausible folding intermediates. The simulations *per se* do not allow for drawing definite conclusions as for whether hemin shifts the equilibrium of various G4 topologies towards the parallel-stranded form, but experimental evidence suggests that porphyrinic ligands indeed favor the parallel-stranded topologies.[104-106] Here, we propose that hemin (and

similar ligands) promotes the parallel-stranded G4 folding by increasing the folding rate of the complete G4 from slip-stranded intermediates. It stabilizes these late-stage folding species and decreases their unfolding rate. These processes could stabilize folding funnel of the parallel-stranded G4 relatively to other G4 folds upon flat ligand binding. However, it should be noted that the MD simulations presented here provide neither complete nor fully accurate description of the G4 systems. Thus, limitations stemming from the nature of the force field and sampling limits must be taken into account during interpretation of the results (further discussed in Supporting Information).[39, 101, 107] However, the possibility that hemin binding contributes to overall stabilization of the parallel-stranded topology also by favorable interactions with its on-pathway folding intermediates seems plausible. The simulations should be accurate enough to reflect relative structural stabilities and rearrangement propensities of the different studied structures.

CONCLUSIONS

We provided an atomistic description of G4/hemin interactions, describing how hemin binds to G4s and how it could affect its folding and its catalytic properties. We observed multiple routes through which hemin binds to G4s, happening either directly to solvent-exposed terminal G-quartets or *via* loop-mediated transfer to the G-quartet (Figures 3, S2 and S3, Supporting Movie SM1). Bases of three-nucleotide loops may further stack to quartet-bound hemin, forming a sandwich-like structure base/hemin/G-stem (Figure 4B).

While acknowledging the simulation limitations, we identified multiple dynamically occurring structures that could contribute to the catalytic activity of G4/hemin DNAzyme, all of which requiring directly or indirectly a G-quartet. Reaction rate enhancement could be related to hemin that is fully stacked atop terminal G-quartets of the folded parallel-stranded G4s, as thermal fluctuations of hemin often sample positions with iron atom around G's O6 atoms, with hemin center somewhat slid off the center of the G-stem (Figure 4A). This dynamics is not apparent from ensemble-averaged data. Alternatively, mere stacking of hemin to the electron-rich aromatic surface of the G-quartet could *per se* enhance the reactivity. Models with a buried water molecule or wobbling G are not supported by the presented simulations.

Our results also offer new insights how loops and flanking bases could enhance the rate of peroxidase reaction *via* the transient formation of base/hemin/G4 sandwich structures (Figure 4B), which supports the model in which the base can interact with H_2O_2 in the vicinity of the hemin iron atom and promote the proton transfer. We finally show that hemin may facilitate the folding of parallel-stranded G4s from slip-stranded G4 intermediates, driving strand slippage in the direction of a complete G4 (Figure 5; Supporting Movie SM2), thus acting as a G4 chaperone. This might have important consequences *in vivo* as G4/hemin interaction is likely to occur in cells. We believe that the characteristics of the G4/hemin systems described here are intrinsic properties that could guide further experimental studies.

ACKNOWLEDGMENTS

This work was supported by the project SYMBIT [CZ.02.1.01/0.0/0.0/15_003/0000477] financed by the European Regional Development Fund with financial contribution from the MEYS CR; J.S. acknowledges support by Praemium Academiae; P.S. greatly appreciates access to storage facilities supplied by the project "e-Infrastruktura CZ" [e-INFRA LM2018140] provided within the program Projects of Large Research, Development and Innovations Infrastructures; J.Z. acknowledges the financial support of the National Natural Science Foundation of China [21977045]; and Fundamental Research Funds for the Central Universities [02051430210]; J.L.M. the funds of Nanjing University [020514912216]; and

D.M. the Agence Nationale de la Recherche [ANR-18-CE07-0017-03]; and the European Union [PO FEDER-FSE Bourgogne 2014/2020 programs].

REFERENCES

(1) Rhodes, D.; Lipps, H. J., G-Quadruplexes and Their Regulatory Roles in Biology. *Nucleic Acids Res.* **2015**, *43*, 8627-8637.

(2) Varshney, D.; Spiegel, J.; Zyner, K.; Tannahill, D.; Balasubramanian, S., The Regulation and Functions of DNA and RNA G-Quadruplexes. *Nat. Rev. Mol. Cell Biol.* **2020**, *21*, 459-474.

(3) Stefan, L.; Monchaud, D., Applications of Guanine Quartets in Nanotechnology and Chemical Biology. *Nat. Rev. Chem.* **2019**, *3*, 650-668.

(4) da Silva, M. W., Geometric Formalism for DNA Quadruplex Folding. *Chem. Eur. J.* **2007**, *13*, 9738-9745.

(5) Karsisiotis, A. I.; O'Kane, C.; da Silva, M. W., DNA Quadruplex Folding Formalism - A Tutorial on Quadruplex Topologies. *Methods* **2013**, *64*, 28-35.

(6) Dvorkin, S. A.; Karsisiotis, A. I.; Webba da Silva, M., Encoding Canonical DNA Quadruplex Structure. *Sci. Adv.* **2018**, *4*, eaat3007.

(7) Chambers, V. S.; Marsico, G.; Boutell, J. M.; Di Antonio, M.; Smith, G. P.; Balasubramanian, S., High-Throughput Sequencing of DNA G-Quadruplex Structures in the Human Genome. *Nat. Biotech.* **2015**, *33*, 877-881.

(8) Bedrat, A.; Lacroix, L.; Mergny, J.-L., Re-Evaluation of G-Quadruplex Propensity with G4Hunter. *Nucleic Acids Res.* **2016**, *44*, 1746-1759.

(9) Hansel-Hertsch, R.; Di Antonio, M.; Balasubramanian, S., DNA G-Quadruplexes in the Human Genome: Detection, Functions and Therapeutic Potential. *Nat. Rev. Mol. Cell Biol.* **2017**, *18*, 279-284.

(10) Graziella, C.-R.; Nadia, Z.; Marco, F., Emerging Role of G-Quadruplex DNA as Target in Anticancer Therapy. *Curr. Pharm. Des.* **2016**, *22*, 6612-6624.

(11) Tateishi-Karimata, H.; Kawauchi, K.; Sugimoto, N., Destabilization of DNA G-Quadruplexes by Chemical Environment Changes during Tumor Progression Facilitates Transcription. *J. Am. Chem. Soc.* **2018**, *140*, 642-651.

(12) Maizels, N., G4-Associated Human Diseases. *EMBO Rep.* **2015**, *16*, 910-922.

(13) Balendra, R.; Isaacs, A. M., C9orf72-Mediated ALS and FTD: Multiple Pathways to Disease. *Nat. Rev. Neurol.* **2018**, *14*, 544-558.

(14) Neidle, S., Quadruplex Nucleic Acids as Novel Therapeutic Targets. *J. Med. Chem.* **2016**, *59*, 5987-6011.

(15) Travascio, P.; Li, Y.; Sen, D., DNA-Enhanced Peroxidase Activity of a DNA Aptamer-Hemin Complex *Chem. Biol.* **1998**, *5*, 505-517.

(16) Morrison, D.; Rothenbroker, M.; Li, Y., DNAzymes: Selected for Applications. *Small Methods* **2018**, *2*, 1700319.

(17) Hollenstein, M., Nucleic Acid Enzymes Based on Functionalized Nucleosides. *Curr. Opin. Chem. Biol.* **2019**, *52*, 93-101.

(18) Mergny, J.-L.; Sen, D., DNA Quadruple Helices in Nanotechnology. *Chem. Rev.* **2019**, *119*, 6290-6325.

(19) Ma, L. Z.; Liu, J. W., Catalytic Nucleic Acids: Biochemistry, Chemical Biology, Biosensors, and Nanotechnology. *iScience* **2020**, *23*, 100815.

(20) Grigg, J. C.; Shumayrikh, N.; Sen, D., G-Quadruplex Structures Formed by Expanded Hexanucleotide Repeat RNA and DNA from the Neurodegenerative Disease-Linked C9orf72 Gene Efficiently Sequester and Activate Heme. *PLoS One* **2014**, *9*, e106449.

(21) Gray, L. T.; Puig Lombardi, E.; Verga, D.; Nicolas, A.; Teulade-Fichou, M.-P.; Londono-Vallejo, A.; Maizels, N., G-Quadruplexes Sequester Free Heme in Living Cells. *Cell Chem. Biol.* **2019**, *26*, 1681-1691.
(22) Mikuma, T.; Ohyama, T.; Terui, N.; Yamamoto, Y.; Hori, H., Coordination Complex Between Haemin and Parallel-Quadruplexed d(TTAGGG). *Chem. Commun.* **2003**, 1708-1709.
(23) Saito, K.; Tai, H.; Hemmi, H.; Kobayashi, N.; Yamamoto, Y., Interaction between the Heme and a G-Quartet in a Heme–DNA Complex. *Inorg. Chem.* **2012**, *51*, 8168-8176.
(24) Shimizu, H.; Tai, H.; Saito, K.; Shibata, T.; Kinoshita, M.; Yamamoto, Y., Characterization of the Interaction between Heme and a Parallel G-Quadruplex DNA Formed from d(TTAGGGT). *Bull. Chem. Soc. Jpn.* **2015**, *88*, 644-652.
(25) Shinomiya, R.; Araki, H.; Momotake, A.; Kotani, H.; Kojima, T.; Yamamoto, Y., Identification of Intermediates in Peroxidase Catalytic Cycle of a DNAzyme Possessing Heme. *Bull. Chem. Soc. Jpn.* **2019**, *92*, 1729-1736.
(26) Shinomiya, R.; Katahira, Y.; Araki, H.; Shibata, T.; Momotake, A.; Yanagisawa, S.; Ogura, T.; Suzuki, A.; Neya, S.; Yamamoto, Y., Characterization of Catalytic Activities and Heme Coordination Structures of Heme–DNA Complexes Composed of Some Chemically Modified Hemes and an All Parallel-Stranded Tetrameric G-Quadruplex DNA Formed from d(TTAGGG). *Biochemistry* **2018**, *57*, 5930-5937.
(27) Yamamoto, Y.; Kinoshita, M.; Katahira, Y.; Shimizu, H.; Di, Y.; Shibata, T.; Tai, H.; Suzuki, A.; Neya, S., Characterization of Heme–DNA Complexes Composed of Some Chemically Modified Hemes and Parallel G-Quadruplex DNAs. *Biochemistry* **2015**, *54*, 7168-7177.
(28) Hayasaka, K.; Shibata, T.; Sugahara, A.; Momotake, A.; Matsui, T.; Neya, S.; Ishizuka, T.; Xu, Y.; Yamamoto, Y., Characterization of Structure and Catalytic Activity of a Complex between Heme and an All Parallel-Stranded Tetrameric G-Quadruplex Formed from DNA/RNA Chimera Sequence d(TTA)r(GGG)dT. *Bull. Chem. Soc. Jpn.* **2020**, *93*, 621-629.
(29) Yamamoto, Y.; Araki, H.; Shinomiya, R.; Hayasaka, K.; Nakayama, Y.; Ochi, K.; Shibata, T.; Momotake, A.; Ohyama, T.; Hagihara, M., et al., Structures and Catalytic Activities of Complexes between Heme and All Parallel-Stranded Monomeric G-Quadruplex DNAs. *Biochemistry* **2018**, *57*, 5938-5948.
(30) Travascio, P.; Witting, P. K.; Mauk, A. G.; Sen, D., The Peroxidase Activity of a Hemin−DNA Oligonucleotide Complex: Free Radical Damage to Specific Guanine Bases of the DNA. *J. Am. Chem. Soc.* **2001**, *123*, 1337-1348.
(31) Chen, J.; Zhang, Y.; Cheng, M.; Guo, Y.; Sponer, J.; Monchaud, D.; Mergny, J.-L.; Ju, H.; Zhou, J., How Proximal Nucleobases Regulate the Catalytic Activity of G-Quadruplex/Hemin DNAzymes. *ACS Catal.* **2018**, *8*, 11352-11361.
(32) Li, W.; Li, Y.; Liu, Z.; Lin, B.; Yi, H.; Xu, F.; Nie, Z.; Yao, S., Insight into G-Quadruplex-Hemin DNAzyme/RNAzyme: Adjacent Adenine as the Intramolecular Species for Remarkable Enhancement of Enzymatic Activity. *Nucleic Acids Res.* **2016**, *44*, 7373-7384.
(33) Chang, T.; Gong, H.; Ding, P.; Liu, X.; Li, W.; Bing, T.; Cao, Z.; Shangguan, D., Activity Enhancement of G-Quadruplex/Hemin DNAzyme by Flanking d(CCC). *Chem. Eur. J.* **2016**, *22*, 4015-4021.
(34) Chen, J.; Guo, Y.; Zhou, J.; Ju, H., The Effect of Adenine Repeats on G-quadruplex/hemin Peroxidase Mimicking DNAzyme Activity. *Chem. Eur. J.* **2017**, *23*, 4210-4215.
(35) Cao, Y.; Ding, P.; Yang, L.; Li, W.; Luo, Y.; Wang, J.; Pei, R., Investigation and Improvement of Catalytic Activity of G-Quadruplex/Hemin DNAzymes Using Designed Terminal G-Tetrads with Deoxyadenosine Caps. *Chem. Sci.* **2020**, *11*, 6896-6906.

(36) Stefan, L.; Denat, F.; Monchaud, D., Insights into How Nucleotide Supplements Enhance the Peroxidase-Mimicking DNAzyme Activity of the G-Quadruplex/Hemin System. *Nucleic Acids Res.* **2012**, *40*, 8759-8772.
(37) Kong, D.-M.; Xu, J.; Shen, H.-X., Positive Effects of ATP on G-Quadruplex-Hemin DNAzyme-Mediated Reactions. *Anal. Chem.* **2010**, *82*, 6148-6153.
(38) Bessi, I.; Jonker, H. R. A.; Richter, C.; Schwalbe, H., Involvement of Long-Lived Intermediate States in the Complex Folding Pathway of the Human Telomeric G-Quadruplex. *Angew. Chem., Int. Ed.* **2015**, *54*, 8444-8448.
(39) Sponer, J.; Bussi, G.; Stadlbauer, P.; Kuhrova, P.; Banas, P.; Islam, B.; Haider, S.; Neidle, S.; Otyepka, M., Folding of Guanine Quadruplex Molecules–Funnel-Like Mechanism or Kinetic Partitioning? An Overview from MD Simulation Studies. *Biochim. Biophys. Acta, Gen. Subj.* **2017**, *1861*, 1246-1263.
(40) Thirumalai, D.; Klimov, D. K.; Woodson, S. A., Kinetic Partitioning Mechanism as a Unifying Theme in the Folding of Biomolecules. *Theor. Chem. Acc.* **1997**, *96*, 14-22.
(41) Long, X.; Stone, M. D., Kinetic Partitioning Modulates Human Telomere DNA G-Quadruplex Structural Polymorphism. *PLoS One* **2013**, *8*, e83420.
(42) Sponer, J.; Islam, B.; Stadlbauer, P.; Haider, S., Chapter Seven - Molecular dynamics simulations of G-quadruplexes: The basic principles and their application to folding and ligand binding. In *Annual Reports in Medicinal Chemistry*, Neidle, S., Ed. Academic Press: 2020; Vol. 54, pp 197-241.
(43) Stadlbauer, P.; Kuhrova, P.; Vicherek, L.; Banas, P.; Otyepka, M.; Trantirek, L.; Sponer, J., Parallel G-Triplexes and G-Hairpins As Potential Transitory Ensembles in the Folding of Parallel-Stranded DNA G-Quadruplexes. *Nucleic Acids Res.* **2019**, *47*, 7276-7293.
(44) Gabelica, V., A Pilgrim's Guide to G-Quadruplex Nucleic Acid Folding. *Biochimie* **2014**, *105*, 1-3.
(45) Aznauryan, M.; Søndergaard, S.; Noer, S. L.; Schiøtt, B.; Birkedal, V., A Direct View of the Complex Multi-Pathway Folding of Telomeric G-Quadruplexes. *Nucleic Acids Res.* **2016**, *44*, 11024-11032.
(46) Marchand, A.; Gabelica, V., Folding and Misfolding Pathways of G-Quadruplex DNA. *Nucleic Acids Res.* **2016**, *44*, 10999-11012.
(47) Xue, Y.; Liu, J.-Q.; Zheng, K.-W.; Kan, Z.-Y.; Hao, Y.-H.; Tan, Z., Kinetic and Thermodynamic Control of G-Quadruplex Folding. *Angew. Chem., Int. Ed.* **2011**, *50*, 8046-8050.
(48) Gray, R. D.; Trent, J. O.; Chaires, J. B., Folding and Unfolding Pathways of the Human Telomeric G-Quadruplex. *J. Mol. Biol.* **2014**, *426*, 1629-1650.
(49) Rajendran, A.; Endo, M.; Hidaka, K.; Teulade-Fichou, M.-P.; Mergny, J.-L.; Sugiyama, H., Small Molecule Binding to a G-hairpin and a G-triplex: A New Insight into Anticancer Drug Design Targeting G-rich Regions. *Chem. Commun.* **2015**, *51*, 9181-9184.
(50) O'Hagan, M. P.; Morales, J. C.; Galan, M. C., Binding and Beyond: What Else Can G-Quadruplex Ligands Do? *Eur. J. Org. Chem.* **2019**, *2019*, 4995-5017.
(51) Stefl, R.; Cheatham, T. E.; Spackova, N.; Fadrna, E.; Berger, I.; Koca, J.; Sponer, J., Formation Pathways of a Guanine-Quadruplex DNA Revealed by Molecular Dynamics and Thermodynamic Analysis of the Substates. *Biophys. J.* **2003**, *85*, 1787-1804.
(52) Stadlbauer, P.; Krepl, M.; Cheatham, T. E., 3rd; Koca, J.; Sponer, J., Structural Dynamics of Possible Late-Stage Intermediates in Folding of Quadruplex DNA Studied by Molecular Simulations. *Nucleic Acids Res.* **2013**, *41*, 7128-7143.
(53) Rocca, R.; Palazzesi, F.; Amato, J.; Costa, G.; Ortuso, F.; Pagano, B.; Randazzo, A.; Novellino, E.; Alcaro, S.; Moraca, F., et al., Folding Intermediate States of the Parallel Human Telomeric G-Quadruplex DNA Explored Using Well-Tempered Metadynamics. *Sci. Rep.* **2020**, *10*, 3176.

(54) Bardin, C.; Leroy, J. L., The Formation Pathway of Tetramolecular G-Quadruplexes. *Nucleic Acids Res.* **2008**, *36*, 477-488.
(55) Mitra, J.; Makurath, M. A.; Ngo, T. T. M.; Troitskaia, A.; Chemla, Y. R.; Ha, T., Extreme Mechanical Diversity of Human Telomeric DNA Revealed by Fluorescence-Force Spectroscopy. *Proc. Natl. Acad. Sci. U. S. A.* **2019**, *116*, 8350-8359.
(56) Gruen, J. T.; Hennecker, C.; Kloetzner, D.-P.; Harkness, R. W.; Bessi, I.; Heckel, A.; Mittermaier, A. K.; Schwalbe, H., Conformational Dynamics of Strand Register Shifts in DNA G-Quadruplexes. *J. Am. Chem. Soc.* **2020**, *142*, 264-273.
(57) Neidle, S., The Structures of Quadruplex Nucleic Acids And Their Drug Complexes. *Curr. Opin. Struct. Biol.* **2009**, *19*, 239-250.
(58) Zhang, S.; Wu, Y.; Zhang, W., G-Quadruplex Structures and Their Interaction Diversity with Ligands. *ChemMedChem* **2014**, *9*, 899-911.
(59) Parkinson, G. N.; Lee, M. P. H.; Neidle, S., Crystal Structure of Parallel Quadruplexes from Human Telomeric DNA. *Nature* **2002**, *417*, 876-880.
(60) Trajkovski, M.; da Silva, M. W.; Plavec, J., Unique Structural Features of Interconverting Monomeric and Dimeric G-quadruplexes Adopted by a Sequence from the Intron of the N-myc Gene. *J. Am. Chem. Soc.* **2012**, *134*, 4132-4141.
(61) Berendsen, H. J. C.; Grigera, J. R.; Straatsma, T. P., The Missing Term in Effective Pair Potentials. *J. Phys. Chem.* **1987**, *91*, 6269-6271.
(62) Joung, I. S.; Cheatham, T. E., Determination of Alkali and Halide Monovalent Ion Parameters for Use In Explicitly Solvated Biomolecular Simulations. *J. Phys. Chem. B* **2008**, *112*, 9020-9041.
(63) Zgarbova, M.; Sponer, J.; Otyepka, M.; Cheatham, T. E.; Galindo-Murillo, R.; Jurecka, P., Refinement of the Sugar–Phosphate Backbone Torsion Beta for AMBER Force Fields Improves the Description of Z- and B-DNA. *J. Chem. Theory Comput.* **2015**, *11*, 5723-5736.
(64) Perez, A.; Marchan, I.; Svozil, D.; Sponer, J.; Cheatham, T. E.; Laughton, C. A.; Orozco, M., Refinement of the AMBER Force Field for Nucleic Acids: Improving the Description of Alpha/Gamma Conformers. *Biophys. J.* **2007**, *92*, 3817-3829.
(65) Krepl, M.; Zgarbova, M.; Stadlbauer, P.; Otyepka, M.; Banas, P.; Koca, J.; Cheatham, T. E.; Jurecka, P.; Sponer, J., Reference Simulations of Noncanonical Nucleic Acids with Different Chi Variants of the AMBER Force Field: Quadruplex DNA, Quadruplex RNA, and Z-DNA. *J. Chem. Theory Comput.* **2012**, *8*, 2506-2520.
(66) Zgarbova, M.; Luque, F. J.; Sponer, J.; Cheatham, T. E.; Otyepka, M.; Jurecka, P., Toward Improved Description of DNA Backbone: Revisiting Epsilon and Zeta Torsion Force Field Parameters. *J. Chem. Theory Comput.* **2013**, *9*, 2339-2354.
(67) Cornell, W. D.; Cieplak, P.; Bayly, C. I.; Gould, I. R.; Merz, K. M.; Ferguson, D. M.; Spellmeyer, D. C.; Fox, T.; Caldwell, J. W.; Kollman, P. A., A Second Generation Force Field for the Simulation of Proteins, Nucleic Acids, and Organic Molecules. *J. Am. Chem. Soc.* **1995**, *117*, 5179-5197.
(68) Wang, J. M.; Cieplak, P.; Kollman, P. A., How Well Does a Restrained Electrostatic Potential (RESP) Model Perform in Calculating Conformational Energies of Organic and Biological Molecules? *J. Comput. Chem.* **2000**, *21*, 1049-1074.
(69) Havrila, M.; Stadlbauer, P.; Islam, B.; Otyepka, M.; Sponer, J., Effect of Monovalent Ion Parameters on Molecular Dynamics Simulations of G-Quadruplexes. *J. Chem. Theory Comput.* **2017**, *13*, 3911-3926.
(70) Shahrokh, K.; Orendt, A.; Yost, G. S.; Cheatham, T. E., Quantum Mechanically Derived AMBER-Compatible Heme Parameters for Various States of the Cytochrome P450 Catalytic Cycle. *J. Comput. Chem.* **2012**, *33*, 119-133.

(71) Case, D. A.; Betz, R. M.; Botello-Smith, W.; Cerutti, D. S.; T.E. Cheatham, I.; Darden, T. A.; Duke, R. E.; Giese, T. J.; Gohlke, H.; Goetz, A. W., et al. *AMBER 2016*, University of California: San Francisco, CA, 2016.
(72) Le Grand, S.; Goetz, A. W.; Walker, R. C., SPFP: Speed Without Compromise - A Mixed Precision Model for GPU Accelerated Molecular Dynamics Simulations. *Comput. Phys. Commun.* **2013**, *184*, 374-380.
(73) Salomon-Ferrer, R.; Goetz, A. W.; Poole, D.; Le Grand, S.; Walker, R. C., Routine Microsecond Molecular Dynamics Simulations with AMBER on GPUs. 2. Explicit Solvent Particle Mesh Ewald. *J. Chem. Theory Comput.* **2013**, *9*, 3878-3888.
(74) Ryckaert, J. P.; Ciccotti, G.; Berendsen, H. J. C., Numerical Integration of Cartesian Equations of Motion of a System with Constraints - Molecular Dynamics of N-alkans. *J. Comput. Phys.* **1977**, *23*, 327-341.
(75) Miyamoto, S.; Kollman, P. A., Settle: An Analytical Version of the SHAKE and RATTLE Algorithm for Rigid Water Models. *J. Comput. Chem.* **1992**, *13*, 952-962.
(76) Hopkins, C. W.; Le Grand, S.; Walker, R. C.; Roitberg, A. E., Long-Time-Step Molecular Dynamics through Hydrogen Mass Repartitioning. *J. Chem. Theory Comput.* **2015**, *11*, 1864-1874.
(77) Darden, T.; York, D.; Pedersen, L., Particle Mesh Ewald - An N.log(N) Method for Ewald Sums in Large Systems. *J. Chem. Phys.* **1993**, *98*, 10089-10092.
(78) Essmann, U.; Perera, L.; Berkowitz, M. L.; Darden, T.; Lee, H.; Pedersen, L. G., A Smooth Particle Mesh Ewald Method. *J. Chem. Phys.* **1995**, *103*, 8577-8593.
(79) Berendsen, H. J. C.; Postma, J. P. M.; Vangunsteren, W. F.; Dinola, A.; Haak, J. R., Molecular-Dynamics with Coupling to an External Bath. *J. Chem. Phys.* **1984**, *81*, 3684-3690.
(80) Islam, B.; Stadlbauer, P.; Vorlickova, M.; Mergny, J.-L.; Otyepka, M.; Sponer, J., Stability of Two-quartet G-quadruplexes and Their Dimers in Atomistic Simulations. *J. Chem. Theory Comput.* **2020**, *16*, 3447-3463.
(81) Cang, X. H.; Sponer, J.; Cheatham, T. E., Explaining the Varied Glycosidic Conformational, G-Tract Length and Sequence Preferences for Anti-Parallel G-Quadruplexes. *Nucleic Acids Res.* **2011**, *39*, 4499-4512.
(82) Sponer, J.; Mladek, A.; Spackova, N.; Cang, X. H.; Cheatham, T. E.; Grimme, S., Relative Stability of Different DNA Guanine Quadruplex Stem Topologies Derived Using Large-Scale Quantum-Chemical Computations. *J. Am. Chem. Soc.* **2013**, *135*, 9785-9796.
(83) Islam, B.; Stadlbauer, P.; Neidle, S.; Haider, S.; Sponer, J., Can We Execute Reliable MM-PBSA Free Energy Computations of Relative Stabilities of Different Guanine Quadruplex Folds? *J. Phys. Chem. B* **2016**, *120*, 2899-2912.
(84) Sabater, L.; Fang, P.-J.; Chang, C.-F.; De Rache, A.; Prado, E.; Dejeu, J.; Garofalo, A.; Lin, J.-H.; Mergny, J.-L.; Defrancq, E., et al., Cobalt(iii)Porphyrin to Target G-Quadruplex DNA. *Dalton Trans.* **2015**, *44*, 3701-3707.
(85) Gkionis, K.; Kruse, H.; Platts, J. A.; Mladek, A.; Koca, J.; Sponer, J., Ion Binding to Quadruplex DNA Stems. Comparison of MM and QM Descriptions Reveals Sizable Polarization Effects Not Included in Contemporary Simulations. *J. Chem. Theory Comput.* **2014**, *10*, 1326-1340.
(86) Campbell, N. H.; Karim, N. H. A.; Parkinson, G. N.; Gunaratnam, M.; Petrucci, V.; Todd, A. K.; Vilar, R.; Neidle, S., Molecular Basis of Structure–Activity Relationships between Salphen Metal Complexes and Human Telomeric DNA Quadruplexes. *J. Med. Chem.* **2012**, *55*, 209-222.
(87) Shumayrikh, N.; Huang, Y. C.; Sen, D., Heme Activation by DNA: Isoguanine Pentaplexes, but Not Quadruplexes, Bind Heme and Enhance Its Oxidative Activity. *Nucleic Acids Res.* **2015**, *43*, 4191-4201.

(88) Xue, T.; Jiang, S.; Qu, Y.; Su, Q.; Cheng, R.; Dubin, S.; Chiu, C.-Y.; Kaner, R.; Huang, Y.; Duan, X., Graphene-Supported Hemin as a Highly Active Biomimetic Oxidation Catalyst. *Angew. Chem., Int. Ed.* **2012**, *51*, 3822-3825.
(89) Guo, Y.; Deng, L.; Li, J.; Guo, S.; Wang, E.; Dong, S., Hemin−Graphene Hybrid Nanosheets with Intrinsic Peroxidase-like Activity for Label-free Colorimetric Detection of Single-Nucleotide Polymorphism. *ACS Nano* **2011**, *5*, 1282-1290.
(90) Wang, Q.; Xu, N.; Lei, J.; Ju, H., Regulative Peroxidase Activity of DNA-Linked Hemin by Graphene Oxide for Fluorescence DNA Sensing. *Chem. Commun.* **2014**, *50*, 6714-6717.
(91) Song, Y.; Chen, Y.; Feng, L.; Ren, J.; Qu, X., Selective and Quantitative Cancer Cell Detection Using Target-Directed Functionalized Graphene and Its Synergetic Peroxidase-Like Activity. *Chem. Commun.* **2011**, *47*, 4436-4438.
(92) Xu, H.; Yang, Z.; Li, H.; Gao, Z., Hemin-Graphene Derivatives with Increased Peroxidase Activities Restrain Protein Tyrosine Nitration. *Chem. Eur. J.* **2017**, *23*, 17755-17763.
(93) Guo, Y.; Chen, J.; Cheng, M.; Monchaud, D.; Zhou, J.; Ju, H., A Thermophilic Tetramolecular G-Quadruplex/Hemin DNAzyme. *Angew. Chem., Int. Ed.* **2017**, *56*, 16636-16640.
(94) Mulholland, K.; Wu, C., Binding of Telomestatin to a Telomeric G-Quadruplex DNA Probed by All-Atom Molecular Dynamics Simulations with Explicit Solvent. *J. Chem. Inf. Model.* **2016**, *56*, 2093-2102.
(95) Mulholland, K.; Siddiquei, F.; Wu, C., Binding Modes and Pathway of RHPS4 to Human Telomeric G-Quadruplex and Duplex DNA Probed by All-Atom Molecular Dynamics Simulations with Explicit Solvent. *Phys. Chem. Chem. Phys.* **2017**, *19*, 18685-18694.
(96) Sullivan, H.-J.; Readmond, C.; Radicella, C.; Persad, V.; Fasano, T.; Wu, C., Binding of Telomestatin, TMPyP4, BSU6037, and BRACO19 to a Telomeric G-Quadruplex–Duplex Hybrid Probed by All-Atom Molecular Dynamics Simulations with Explicit Solvent. *ACS Omega* **2018**, *3*, 14788-14806.
(97) Machireddy, B.; Sullivan, H.-J.; Wu, C., Binding of BRACO19 to a Telomeric G-Quadruplex DNA Probed by All-Atom Molecular Dynamics Simulations with Explicit Solvent. *Molecules* **2019**, *24*.
(98) Mulholland, K.; Sullivan, H.-J.; Garner, J.; Cai, J.; Chen, B.; Wu, C., Three-Dimensional Structure of RNA Monomeric G-Quadruplex Containing ALS and FTD Related G4C2 Repeat and Its Binding with TMPyP4 Probed by Homology Modeling based on Experimental Constraints and Molecular Dynamics Simulations. *ACS Chem. Neurosci.* **2020**, *11*, 57-75.
(99) Luo, D.; Mu, Y., All-Atomic Simulations on Human Telomeric G-Quadruplex DNA Binding with Thioflavin T. *J. Phys. Chem. B* **2015**, *119*, 4955-4967.
(100) Machireddy, B.; Kalra, G.; Jonnalagadda, S.; Ramanujachary, K.; Wu, C., Probing the Binding Pathway of BRACO19 to a Parallel-Stranded Human Telomeric G-Quadruplex Using Molecular Dynamics Binding Simulation with AMBER DNA OL15 and Ligand GAFF2 Force Fields. *J. Chem. Inf. Model.* **2017**, *57*, 2846-2864.
(101) Sponer, J.; Bussi, G.; Krepl, M.; Banas, P.; Bottaro, S.; Cunha, R. A.; Gil-Ley, A.; Pinamonti, G.; Poblete, S.; Jurecka, P., et al., RNA Structural Dynamics As Captured by Molecular Simulations: A Comprehensive Overview. *Chem. Rev.* **2018**, *118*, 4177-4338.
(102) Havrila, M.; Stadlbauer, P.; Kuhrova, P.; Banas, P.; Mergny, J.-L.; Otyepka, M.; Sponer, J., Structural Dynamics of Propeller Loop: Towards Folding of RNA G-Quadruplex. *Nucleic Acids Res.* **2018**, *46*, 8754-8771.
(103) Cian, A. D.; Mergny, J.-L., Quadruplex Ligands May Act as Molecular Chaperones for Tetramolecular Quadruplex Formation. *Nucleic Acids Res.* **2007**, *35*, 2483-2493.

(104) Nicoludis, J. M.; Barrett, S. P.; Mergny, J.-L.; Yatsunyk, L. A., Interaction of Human Telomeric DNA with N-Methyl Mesoporphyrin IX. *Nucleic Acids Res.* **2012**, *40*, 5432-5447.
(105) Ai, T.; Yang, Q.; Lv, Y.; Huang, Y.; Li, Y.; Geng, J.; Xiao, D.; Zhou, C., Insight into How Telomeric G-Quadruplexes Enhance the Peroxidase Activity of Cellular Hemin. *Chem. - Asian. J.* **2018**, *13*, 1805-1810.
(106) Kong, D.-M.; Yang, W.; Wu, J.; Li, C.-X.; Shen, H.-X., Structure–Function Study of Peroxidase-Like G-Quadruplex-Hemin Complexes. *Analyst* **2010**, *135*, 321-326.
(107) Lemkul, J. A., Same Fold, Different Properties: Polarizable Molecular Dynamics Simulations of Telomeric and TERRA G-Quadruplexes. *Nucleic Acids Res.* **2019**, *48*, 561-575.